Spinal dI2 interneurons regulate the stability of bipedal stepping

Baruch Haimson[1], Yoav Hadas[1], Artur Kania[2], Monica Daley[3], Yuval Cinnamon[4], Aharon Lev-Tov[1,*] and Avihu Klar[1,*]

1 - Department of Medical Neurobiology, IMRIC, Hebrew University-Hadassah Medical School, Jerusalem, 91120, Israel
2 - Institut de recherches cliniques de Montréal (IRCM), Montréal, QC, H2W 1R7, Canada
3 - Ecology and Evolutionary Biology, University of California, Irvine, CA, USA
4 - Institute of Animal Science Poultry and Aquaculture Sci. Dept. Agricultural Research Organization, The Volcani Center, Israel

* - Corresponding authors

Avihu Klar
Department of medical Neurobiology
Hadassah Medical School
The Hebrew University, Jerusalem
91120
Israel
avihu.klar@mail.huji.ac.il

Aharon Lev-Tov
Department of medical Neurobiology
Hadassah Medical School
The Hebrew University, Jerusalem
91120
Israel
aharonl@ekmd.huji.ac.il

Summary

Peripheral and intraspinal feedback is required to shape and update the output of spinal networks that execute motor behavior. We report that lumbar dI2 spinal interneurons of the chick receive synaptic input from afferents and pre-motoneurons. They innervate contralateral premotor networks in the lumbar and brachial spinal cord and their ascending projections innervate the cerebellum. These findings suggest that dI2 neurons function as interneurons in local lumbar circuits and involved in lumbo-brachial coupling and that part of them deliver peripheral and intraspinal feedback to the cerebellum. Silencing of dI2 neurons leads to destabilized stepping in P8 hatchlings with occasional collapses, variable step-profiles and wide-base walking, suggesting that the dI2 neurons may contribute to stabilization of the bipedal gait.

Keywords: spinal cord, spinocerebellar tract, neuronal circuits, locomotion

50 **Introduction**

51 The spinal cord integrates and relays the somatosensory inputs required for further
52 execution of complex motor behaviors. Interneurons that differentiate at the ventral
53 progenitor domain, V3-V0, are involved in the control of rhythmic motor activity, alternating
54 between left and right limbs, as well as between flexor and extensor muscles (Lai et al.,
55 2016, Osseward and Pfaff, 2019, Alaynick et al., 2011). Some of the dorsally born
56 interneurons, dI1, dI3 and dI6, migrate ventrally and are also assembled within circuitry that
57 control motor activity (Yuengert et al., 2015, Bui et al., 2013, Andersson et al., 2012), while
58 other dorsal progenitor neurons, dI4 and dI5, give rise to interneurons that mediate
59 somatosensation (Lai et al., 2016). The role of dI2 neuron is elusive due to the lack of genetic
60 targeting means. Employing intersectional genetics in the chick spinal cord we targeted dI2
61 and present evidences that implicate them in the control of stability during locomotion.

62 The maintenance of stability of the body and the coordination, precision and timing
63 of movements are regulated and modulated by the cerebellum. Anatomical and
64 electrophysiological studies of cats and rodents revealed two major pathways ascending
65 from tract neurons in the lumbar spinal cord to the cerebellum: the dorsal and the ventral
66 spinocerebellar tract (DSCT and VSCT). DSCT tract neurons are considered to relay mainly
67 proprioceptive information, while VSCT tract neurons are thought to relay internal spinal
68 network-information to the cerebellum in addition to proprioceptive data (Jankowska and
69 Hammar, 2013, Spanne and Jorntell, 2013, Stecina et al., 2013, Jiang et al., 2015). While
70 subpopulations of DSCT neuron are genetically accessible (Hantman and Jessell, 2010), the
71 genetic inaccessibility of VSCT neurons hinders revealing their actual contribution to the
72 regulatory functions of the cerebellum in locomotion and other motor behaviors.

In the present study we studied the possible functions of dI2 neurons in chick motor behavior. There are several reasons and advantages to perform these studies in chicks: The patterning of neurons within the spinal cord (Jessell, 2000) and the spinocerebellar tracts (Furue et al., 2010, Furue et al., 2011, Uehara et al., 2012) are conserved between mammalians and avian. In addition, chick uses bipedal locomotion (evolved in humans and birds) that can be examined soon after hatching. For decoding the circuitry and function of spinal interneurons we developed a unique circuit-deciphering toolbox that enables neuronal-specific targeting and tracing of circuits in the chick embryo (Hadas et al., 2014), and utilized kinematic analysis of overground bipedal stepping of the hatched chicks following silencing of dI2.

Our studies revealed that lumbar dI2 neurons receive synaptic inputs from inhibitory and excitatory premotoneurons and relay output to the cerebellar granular layer, premotor neurons at the contralateral spinal cord and the contralateral dI2. Kinematic analysis of overground stepping of P8 hatchlings after Inhibition of the neuronal activity of dI2s by targeted expression of the tetanus toxin gene, showed unstable stepping in the genetically manipulated hatchlings, hence demonstrating that dI2s play a role in shaping and stabilizing the bipedal gait.

90 **Results**

91 In order to define potential VSCT neurons within spinal interneurons, we set the following
92 criteria: 1) Soma location in accordance with pre-cerebellar neurons at the lumbar level,
93 which were previously revealed by retrograde labeling experiments of the chick cerebellar
94 lobes (Furue et al., 2010, Furue et al., 2011, Uehara et al., 2012), 2) Commissural neurons, 3)
95 excitatory neurons, and 4) non-premotoneurons (Lai et al., 2016, Osseward and Pfaff, 2019,
96 Alaynick et al., 2011). Based on these criteria dI1c and dI2 neurons are likely candidates
97 (Bermingham et al., 2001, Yuengert et al., 2015) (Fig. S1B). This is further supported by Sakai
98 et al., who demonstrated that in the E12 chick, dI1 and dI2 axons project to the hindbrain
99 and toward the cerebellum (Sakai et al., 2012). In the current study we have focused on
100 deciphering the circuitry and function of dI2 neurons and their possible association to VSCT.
101

102 **dI2 interneurons are mainly excitatory neurons with commissural axonal projection**

103 The dI2 neurons originate at the dorsal spinal cord. The progenitor pdI2 express Ngn1, Ngn2,
104 Olig3 and Pax3 transcription factors (TFs). The post mitotic dI2 are defined by a
105 combinatorial expression of Foxd3^{+}/Lhx1^{+}/Pou4f1^{+} TFs (Alaynick et al., 2011, Morikawa et
106 al., 2009, Francius et al., 2013). To label dI2 neurons, axons, and terminals in the chick spinal
107 cord we used intersection between enhancers of two dI2's TFs - Ngn1 and the Foxd3, via
108 expression of two recombinases (Cre and FLPo) and double conditional reporters (Fig. S1A).
109 We have shown previously that the combination of these enhancers reliably labels dI2
110 neurons (Avraham et al., 2009, Hadas et al., 2014). At E5, early post mitotic dI2 neurons
111 migrate ventrally from the dorso-lateral to the mid-lateral spinal cord (Fig. 1A). As they
112 migrate ventrally, at E6, dI2 neurons assume a mid-lateral position along the dorso-ventral
113 axis (Fig. 1B). Subsequently, dI2 neurons migrate medially, and at E17, comparable to pos-

114 gestation day 4 (P4) of mouse, they occupy lamina VII (Fig. 1C). At all rostro-caudal levels and
115 embryonic stages, dI2 axons cross the floor plate (Fig. 1A-D). Post-crossing dI2 axons extend
116 rostrally for a few segments at the ventral funiculus (VF) and subsequently turn into the
117 lateral funiculus (LF) (Avraham et al., 2009) (Fig. 1C). The VF to LF rerouting is apparent at
118 the rostral thoracic levels (Fig. 1D). Collaterals originating from the crossed VF and LF tracts
119 invade the contralateral spinal cord (Fig. 1C, D, Fig. 4A,B).

120 A recent study suggested that dI2 neurons at early stages of development in mice at
121 E9.5-E13.5 (comparable the chick E4-8) can be divided into several sub classes based on their
122 genetic signature, and degree of maturation (Delile et al., 2019). To assess the diversity of
123 dI2 neurons in the chick, the expression of dI2 TFs in dI2::GFP cells was analyzed at E5 before
124 and during ventral migration, E6 and E14. The early post mitotic dI2::GFP at E5 are a
125 homogenous population defined by Foxd3^{+}/Lhx1^{+}/Pou4f1^{+}/Pax2^{-} (Fig. 1E, S2A,B). The dI2
126 neurons that undergo ventral migration at E5, as well as at E6 and E14, express variable
127 combinations of Lhx1, Pou4f1 and FoxP1/2/4 (Fig. 1E, S2C,D). At E14, about 50% of dI2::GFP
128 did not express any of the tested TFs (Fig. 1E), suggesting that the early expression of TFs is
129 required for cell fate acquisition, axon guidance, and target recognition, while their
130 expression is redundant during circuitry formation, as shown for other spinal INs (Bikoff et
131 al., 2016). Interestingly, about 12% of ventrally migrating dI2 neurons (from E5 to E14)
132 express Pax2 (Fig. 1E, S2D). Pax2 is associated with an inhibitory phenotype (Cheng et al.,
133 2004), suggesting that a subpopulation of dI2 are inhibitory neurons. The distribution of
134 excitatory and inhibitory dI2 neurons is also apparent at E17. *In situ* hybridization on cross
135 sections of E17 dI2::GFP-labeled lumbar spinal cord, the vGlut2 probe revealed that 88%
136 were vGlut2^{+}, while the Gad1 probe measured 25% Gad1^{+} dI2 neurons (Fig. S3A-D). A similar

137

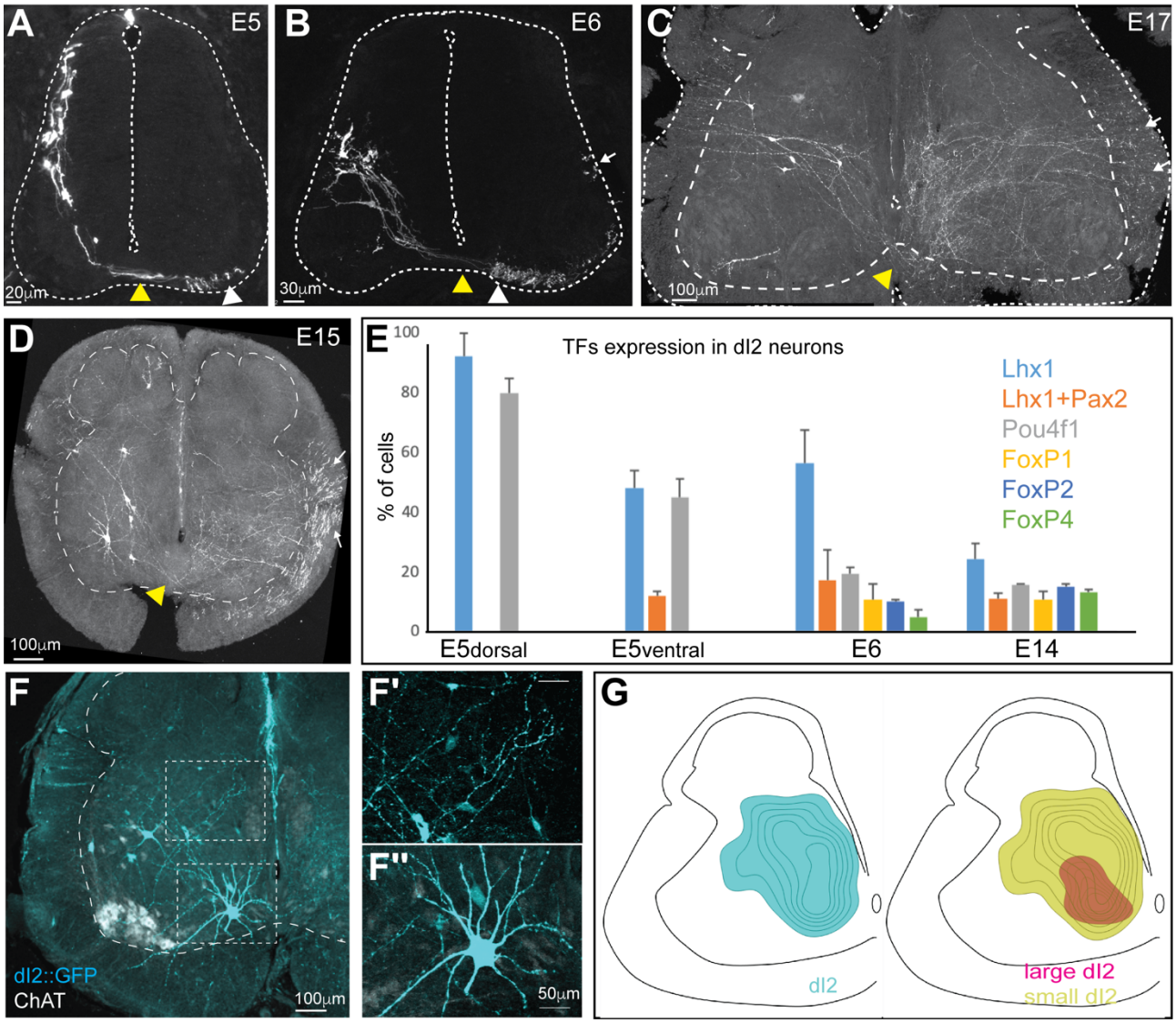

138 Figure 1: Characterization and classification of dI2 neurons during embryonic development.
dI2 interneurons were labeled by genetic intersection between Foxd3 and Ngn1 enhancers (Avraham et al., 2009) (Supp Fig. S1).
A–D. dI2 axonal projection during development. At E5 (A) post mitotic dI2 neurons assume a dorsolateral position and start to migrate ventrally. At E6 (B) dI2 neurons occupy the mid-lateral domain. At E15-17 dI2 neurons are located at the medial lamina VII at the lumbar level (LS3) (C) and the thoracic level (T1) (D). dI2 axons cross the floor plate (yellow arrowheads), turn longitudinally at the ventral funiculus (white arrowheads) and eventually elongate at the lateral funiculus (white arrows).
E. A graph indicating the fraction of dI2 neurons expressing TFs during development (based on data from three E5, two E6 and two E14 embryos). **F.** Cross section of an E17 embryo at the lumbar spinal cord (crural plexus level, LS2). Small-diameter dI2 neurons residing in lamina VII (F') and ventromedial large-diameter dI2 neurons in lamina VIII (F"). **G.** Density plots of dI2 somata in the sciatic plexus level (cyan, *N*=374 cells), $dI2_{large}$ (magenta) and $dI2_{small}$ (yellow) INs (*N*=33 and *N*=344 cells, respectively, from 2 embryos).
See Figure S2 and S3.

139 percentage of Gad2 and Slc6a5 dI2-expressing cells was found also in mouse (Delile et al.,
140 2019). At E13-17 in the caudal lumbar level and at the level of the sciatic plexus, most dI2
141 neurons reside at the medial aspect of lamina VII. About 91% of dI2 neurons are small-
142 diameter neurons that reside at the lateral dorsal aspect of lamina VII, and 9% are large-
143 diameter neurons. At the lumbar sciatic plexus level, large-diameter dI2 neurons mostly
144 reside at the ventral aspect of lamina VII (Fig. 1F,G) and at the level of the crural plexus in
145 the ventral and dorsal aspect of lamina VII (Fig. S3E). Importantly, large-diameter dI2
146 neurons are only apparent at the lumbar level (Fig. 1F, S3E-F). The division of large- and
147 small-diameter lumbar dI2 neurons was not reflected in the expression of the tested TFs.
148 Hence, dI2 neurons consist several sub-populations, as it was shown with other spinal
149 interneurons (Bikoff et al., 2016, Delile et al., 2019, Sweeney et al., 2018)
150

151 **Sub-population of dI2 neurons project to the cerebellum**

152 To study the supraspinal targets of dI2 neurons, axonal and synaptic reporters were
153 expressed in lumbar dI2 neurons (Fig. 2A). At E3, dI2 enhancers were co-electroporated with
154 double conditional axonal reporter – membrane tethered cherry, and synaptic reporter –
155 SV2-GFP (Fig. S1A). Expression into the lumbar spinal cord was attained by using thin
156 electrodes positioned near the lumbar segments. At E17, the stage in which the internal
157 granule layer is formed in the chick cerebellum, the axons and synapses of dI2 neurons were
158 studied. dI2 axons cross the spinal cord at the floor plate at the segmental level, ascend to
159 the cerebellum, enter through the superior cerebellar peduncle, and cross back to the other
160 side of the cerebellum ipsilaterally to the targeted dI2s (Fig. 2B). Synaptic boutons are
161 noticeable in the granule layer at the ipsilateral and contralateral sides of the anterior

162 cerebellar lobules (Fig. 2C). Synaptic boutons were also present in the central cerebellar
163 nuclei (Fig. S4A).

164 The difference in the soma size between the dorsally and ventrally located dI2
165 neurons prompted us to test which dI2 neurons project to the cerebellum. The dI2 and pre-
166 cerebellar neurons were co-labeled by genetic targeting of dI2 at early stages of
167 embryogenesis (E3), coupled with intra-cerebellar injection of cholera toxin subunit B (CTB)
168 or replication-defective HSV-LacZ at E15 (Fig. 2A). Spinal neurons retrogradely-labelled from
169 the cerebellum consist of the double crossed VSCT and the ipsilaterally projecting DSCT
170 neurons. However, dI2 neurons, double labelled by genetic targeting and back labelling from
171 the cerebellum, are all VSCT neurons, since dI2 are commissural neurons. Only the large-
172 diameter neurons were co-labeled, most of them in the ventral aspect of lamina VII (Fig.
173 2D,E,H; S4B,C). Interestingly, many of CTB^+ or $LacZ^+$ neurons were contacted by dI2 axons
174 (Fig. 2F,G,I; S4D,E), suggesting that small-diameter dI2 neurons innervate pre-cerebellar
175 neurons.

176 Segmental crossing at the lumbar level and re-crossing back to the ipsilateral side at
177 the cerebellum, is a characteristic of the VSCT projection pattern. To measure the proportion
178 of dI2 in VSCT neurons, we labeled VSCT axons with GFP and dI2 axons with cherry (for
179 experimental design see Supp. Fig. S4G,F). The number of axons expressing the reporters at
180 the contralateral superior cerebellar peduncle was scored. Ten percent of the VSCT axons
181 belonged to dI2 (Fig. S4H). Thus, the large diameter dI2s are 10% of the VSCT neurons,
182 consistent with the anatomical observation that VSCT comprise a heterogeneous population
183 of interneurons (Jankowska and Hammar, 2013, Stecina et al., 2013).

184

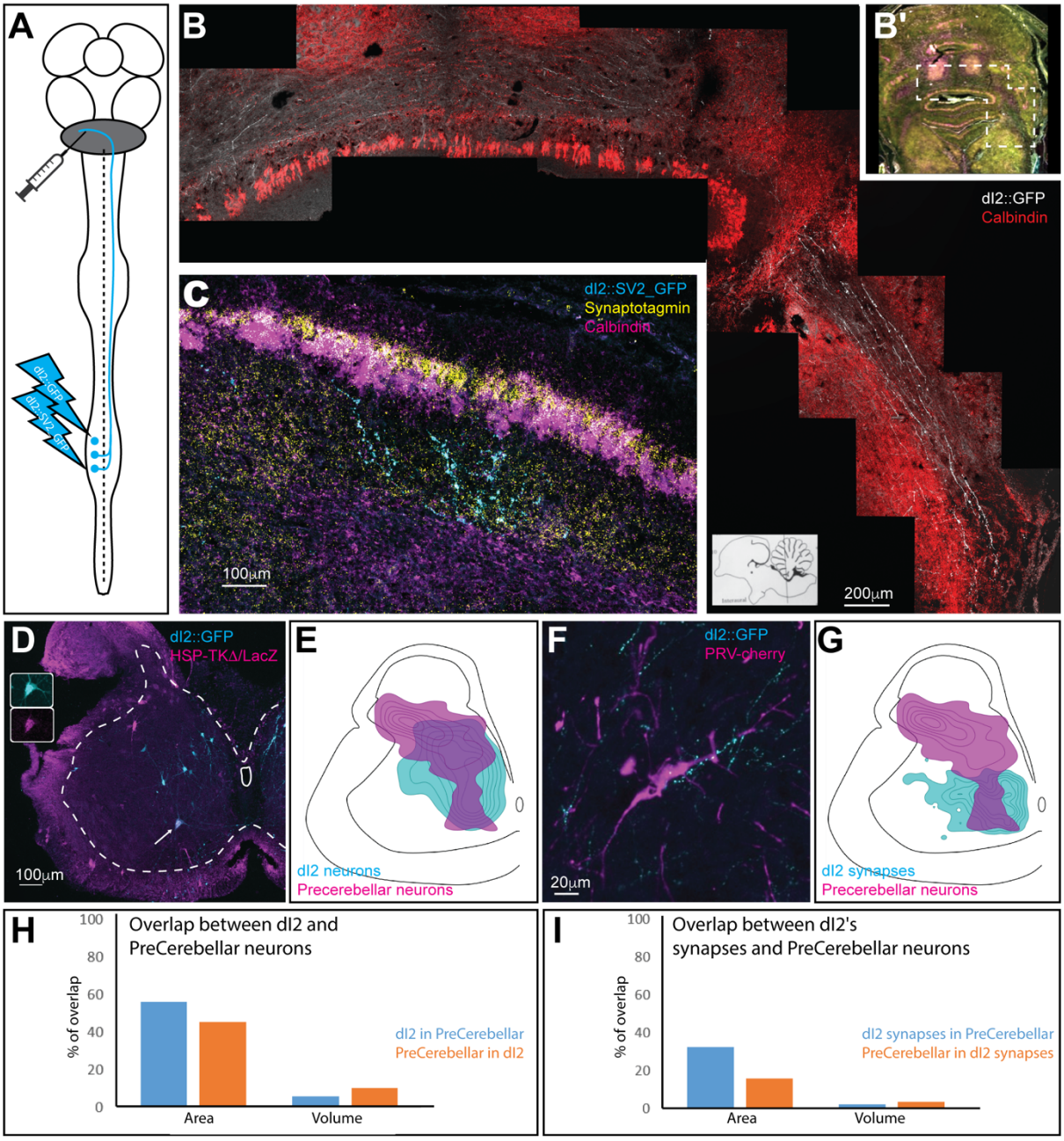

185 Figure 2: dI2 neurons project to the cerebellum.

A. Experimental setup for labeling of cerebellar projecting dI2 neurons. dI2 neurons were genetically targeted at HH18, and pre-cerebellar neurons were labeled using intra-cerebellar injection of CTB or replication defective HSV-LacZ at E15. **B.** A cross section of E17 brainstem and cerebellum. The dashed polygon in B' is magnified in B. dI2 axons reach the cerebellum, enter into it via the superior cerebellar peduncle and cross the cerebellum midline. Calbindin (Purkinje neurons, magenta (B') or red (B)), synaptotagmin (yellow). **C.** A cross section of E17 cerebellar cortex. Lumbar-originating dI2 synapses (cyan) in the granular layer of the anterior cerebellar cortex. Calbindin (Purkinje neurons, magenta), synaptotagmin (yellow). **D.** A cross section of an E15 embryo at the lumbar spinal cord level (sciatic plexus level). Pre-cerebellar neurons were infected and labeled by HSV-LacZ (magenta), and dI2 neurons express GFP (cyan). A large-diameter dI2 neuron co-expressing LacZ and GFP is indicated by an arrow (magnification of the two channels in the insets). **E.** Density plots of dI2 and pre-cerebellar neurons (density values 10-90%) in the sciatic plexus segments (*N*=374 and *N*=289 cells, respectively). **F.** CTB labeled pre-cerebellar neuron (magenta) is contacted by dI2 axonal terminals (cyan). **G.** Density plots of dI2 synapses and pre-cerebellar neuron somata (density values 10-90%) in the sciatic plexus segments (*N*=4735 synapses and *N*=289 cells, respectively). **H,I.** Quantification of the overlap in area and volume of the two density plots. The plots are based on data from 3 embryos. See Figure S4.

186 **dI2 neurons receive synaptic input from pre-motoneurons and sensory neurons**

187 To assess the synaptic input to dI2 neurons we investigated their synaptic connectivity with
188 known pre-VSCT neurons: dorsal root ganglion (DRG) neurons, inhibitory and excitatory pre-
189 motoneurons and reticulospinal tract neurons. Two genetically defined pre-motoneurons
190 were examined: V1 – an inhibitory pre-motoneuronal population (Bikoff et al., 2016,
191 Gosgnach et al., 2006) and dI1i excitatory INs. A density plot of dI1 synapses shows dI1i
192 terminals within the motoneuron pools (lamina IX) and at lamina VII (Fig. 3C). Co-labeling of
193 motoneurons and dI1 synapses revealed synaptic contacts of dI1i on motoneurons (Fig. S5A-
194 B). This was further supported by co-labeling dI1 with pre-MNs via hindlimb injection of
195 pseudorabies virus (PRV) (Fig. S5C-D).

196 To identify neurons presynaptic to dI2 cells we initially assessed the likelihood of
197 connectivity by examining spatial overlap of axonal terminals from the presumed
198 presynaptic neurons and the somata of dI2 neurons, and consequently by detection of
199 synaptic boutons on the somatodendritic membrane of dI2 neurons. We have shown
200 previously that genetic targeting of synaptic reporter in chick spinal cord neurons, yields
201 overlapping expression of the reporter and endogenous pre-synaptic proteins (Hadas et al.,
202 2014). This observation was confirmed using synaptic reporter expressed in dI1 and
203 cytoplasmic reporter expressed in dI2 (Fig. 3C'). The dI2, DRG, V1, and dI1 neurons were
204 labeled using specific enhancers (Fig. S1A). General premotor INs were labeled by injection
205 of PRV-cherry virus into the ipsilateral hindlimb musculature (Hadas et al., 2014) (Fig. 3B).

206 A density profile of the axons of DRG neurons (Fig. 3A, S6A-D) and PRV-labeled pre-
207 MNs (Fig. 3B), and a density profile of synaptic boutons from dI1i (Fig. 3C, S6E), V1 (Fig. 3D),
208 and reticulospinal tract neurons ($5HT^+$ synapses) (Fig. 3E, S6F) were aligned to the density
209 plots of the dI2 somata. The overlap between the axonal terminals of DRG neurons, PRV-

210 labeled pre-motoneurons, dI1i and V1 boutons, and the somata of dI2 neurons is evident
211 (Fig. 3A-F, Fig. S6G). To further substantiate these putative synaptic connections, we
212 performed double labeling of DRG, PRV-labeled pre-motoneurons, V1, and dI1i, together
213 with dI2 neurons. Hindlimb pre-motor neurons were labeled by injection of PRV into the
214 hindlimb musculature (Hadas et al., 2014); DRG and dI1 terminal and synapses by cell-type
215 specific enhancer (Fig. S1A); V1 synapses by a double conditional on/off reporter plasmids
216 that enables activation of synaptic reporter in V1 and dI2 utilizing the Foxd3 enhancer and
217 deletion of the synaptic reporter from dI2 neurons utilizing the Ngn1 enhancer (Fig. S1A).
218 Contact between DRG axons and dI2 neurons was mainly apparent in the dorsal dI2
219 neurons, while the ventral dI2 neurons received little to no input from DRG neurons (Fig. 3A,
220 S6A,B). Synaptic connections, evaluated by boutons on dI2 dendrites and somata, are
221 apparent from the pre-motor neurons V1 and dI1i (Fig. 3C,D). Serotonergic synapses were
222 found to be concentrated on motoneurons and were not observed on dI2 neurons (Fig. 3E,
223 S6F). Double-labeling of 5HT and dI2 neurons did not reveal any synaptic input. The lack of
224 synaptic serotonergic input may be related to the difference in species, or may suggest that
225 other, non-dI2 VSCT neurons residing adjacent to motoneurons, are contacted by the
226 reticulospinal neurons. The analysis of the synaptic inputs supports the concept that dI2
227 neurons constitute part of the VSCT. They receive input from sensory afferents, inhibitory
228 and excitatory pre-motoneurons and project to the cerebellum.

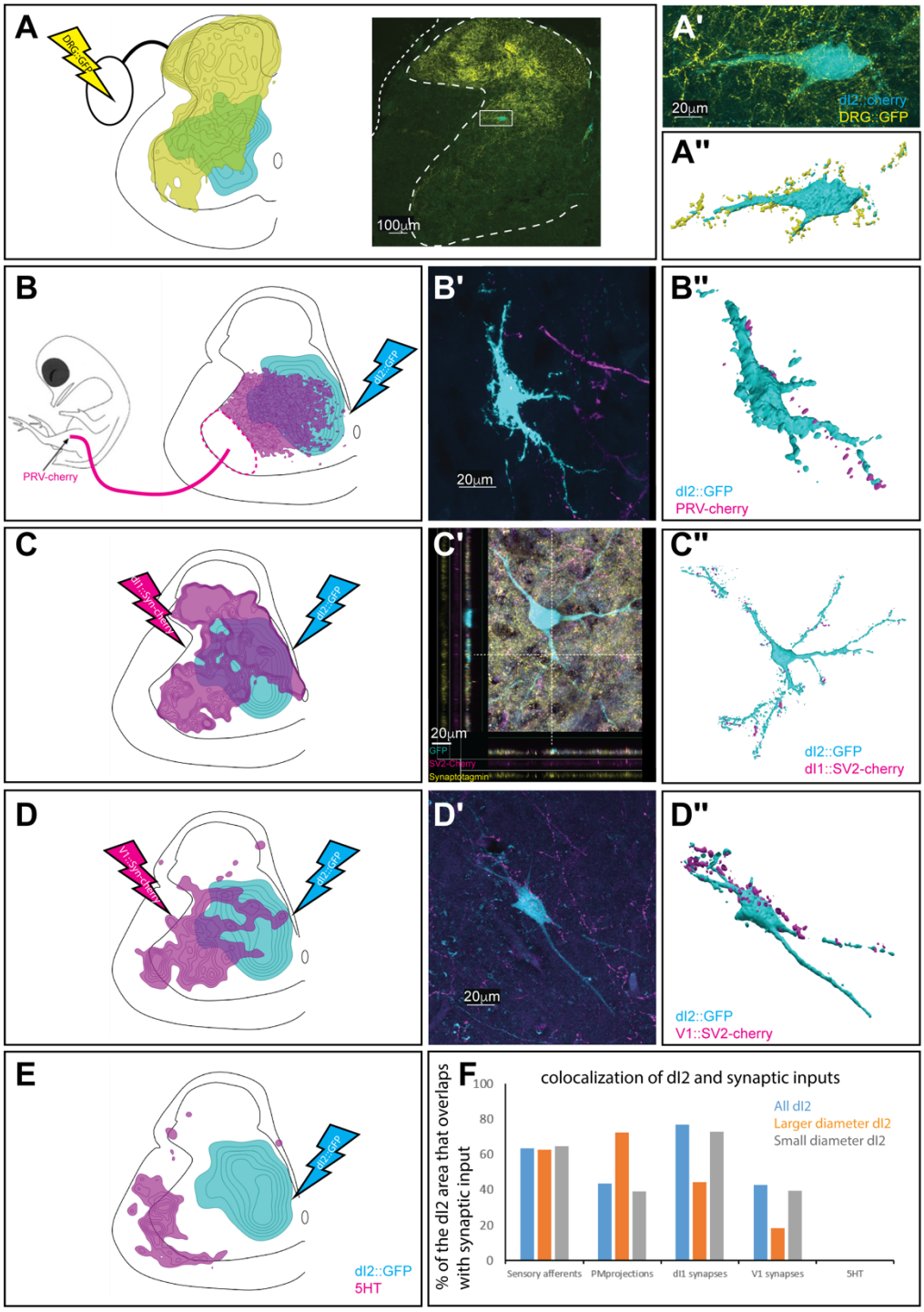

229

Figure 3: Synaptic inputs to dI2 neurons.

Schematic representations of the experimental design for labeling dI2::GFP or dI2::cherry INs (cyan) and potential sources of synaptic inputs (yellow or magenta), supplemented by cell soma density of dI2 INs and the synaptic densities are illustrated in A, B, C, D, E. The density values presented are 10-80%, 20-80%, 25-80%, 30-50% and 20-80%, respectively.

Examples of dI2 neurons contacted by axons or synaptic boutons are shown in A', B', C', and D'; and their 3D reconstruction in A'', B'', C'', and D''. Genetic labeling was attained using specific enhancers (Fig. S1) electroporated at HH18.

A. DRG neurons form contacts on dI2 neurons. Inset in A: cross section of and E17 embryo at the crural plexus level of the lumbar cord. A dorsally located dI2 neuron contacted by numerous sensory afferents, magnified in A' and 3D-reconstructed in A''. (*N*=18 sections)

B. Premotoneurons form contacts on dI2 neurons. dI2 neurons were labeled at HH18. At E13, PRV virus was injected to the leg musculature, and the embryo was incubated until premotoneuronal infection (39 hours) (*N*=34 sections).

C. dI1 neurons form synapses on dI2 neurons. (*N*=8568 synapses). C': A representative SV2::cherry synapse on dI2 dendrite, positive for synaptotagmin. Demonstrated by a horizontal and vertical optical sections in Z-axis (see cursors and color channels).

D. V1 neurons form synapses on dI2 neurons. (*N*=1923 synapses).

E. dI2 neurons do not have 5HT synaptic terminals (*N*=1718 synapses). E17 cross sections of dI2::GFP labeled embryos were stained for 5HT.

F. Quantification of the overlap area of the different input sources and dI2 neuron densities plots. See Figure S5, S6.

231 **dI2 neurons innervate contralateral lumbar and brachial pre-MNs and dI2 neurons**

232 Axon collaterals of dI2 invade the spinal cord gray matter along the entire length of the
233 spinal cord, as revealed by whole mount staining of spinal cords electroporated with alkaline
234 phosphatase reporter (dI2::AP) (Fig. 4A) and membrane-tethered EGFP (Fig. 4B). The region
235 innervated by dI2 collaterals (arrow at Fig. 4B) overlaps with that of the pre-MNs, V0 and V1
236 (Lai et al., 2016, Griener et al., 2015), as well as with that of the contralateral dI2 neurons
237 (Fig. 1, Fig. 4B). To assess the potential spinal targets of dI2 neurons, we scored the degree
238 of overlap between of dI2 synapses and dI2 somata (Fig. 4C), the ipsilateral pre-MNs (Fig.
239 4D), and contralateral pre-MNs (Fig. 4E). The alignment revealed a significant overlap of dI2
240 synapses with ipsi/contralateral pre-MNs and dI2 neurons (Fig. 4G,H). Co-labeling of synaptic
241 dI2 coupled with labeling of the above neuronal population showed dI2 synaptic boutons on
242 pre-MNs and dI2 neurons at the lumbar level (Fig. 4C-H, S7A-C).

243 The pattern of dI2 collaterals along the entire rostrocaudal axis (Fig. 4A) suggests that
244 dI2 neurons innervate contralateral pre-MNs and dI2 neurons at multiple levels. To test this,
245 labeling of lumbar dI2 neurons was coupled with labeling of brachial pre-MNs and dI2 soma
246 labeling via wing musculature injection of PRV or electroporation of reporter in brachial dI2
247 neurons, respectively (Fig. 4F, S7D). dI2-synapses and the putative targets overlapped, and
248 synaptic boutons originated from lumbar level dI2 neurons are apparent on dI2 neurons, and
249 on the contra- and ipsilateral pre-MNs of the wings (Fig. 4F, S7D-F).

250 The neuronal and synaptic labelling experiments showed that lumbar dI2 neurons
251 innervate the cerebellum, lumbar and brachial pre-MN, and contralateral dI2 neurons (Fig.
252 6D). Hence, dI2 neurons may relay peripheral and intraspinal information to the cerebellum
253 and to the contralateral lumbar and brachial motor control centers.

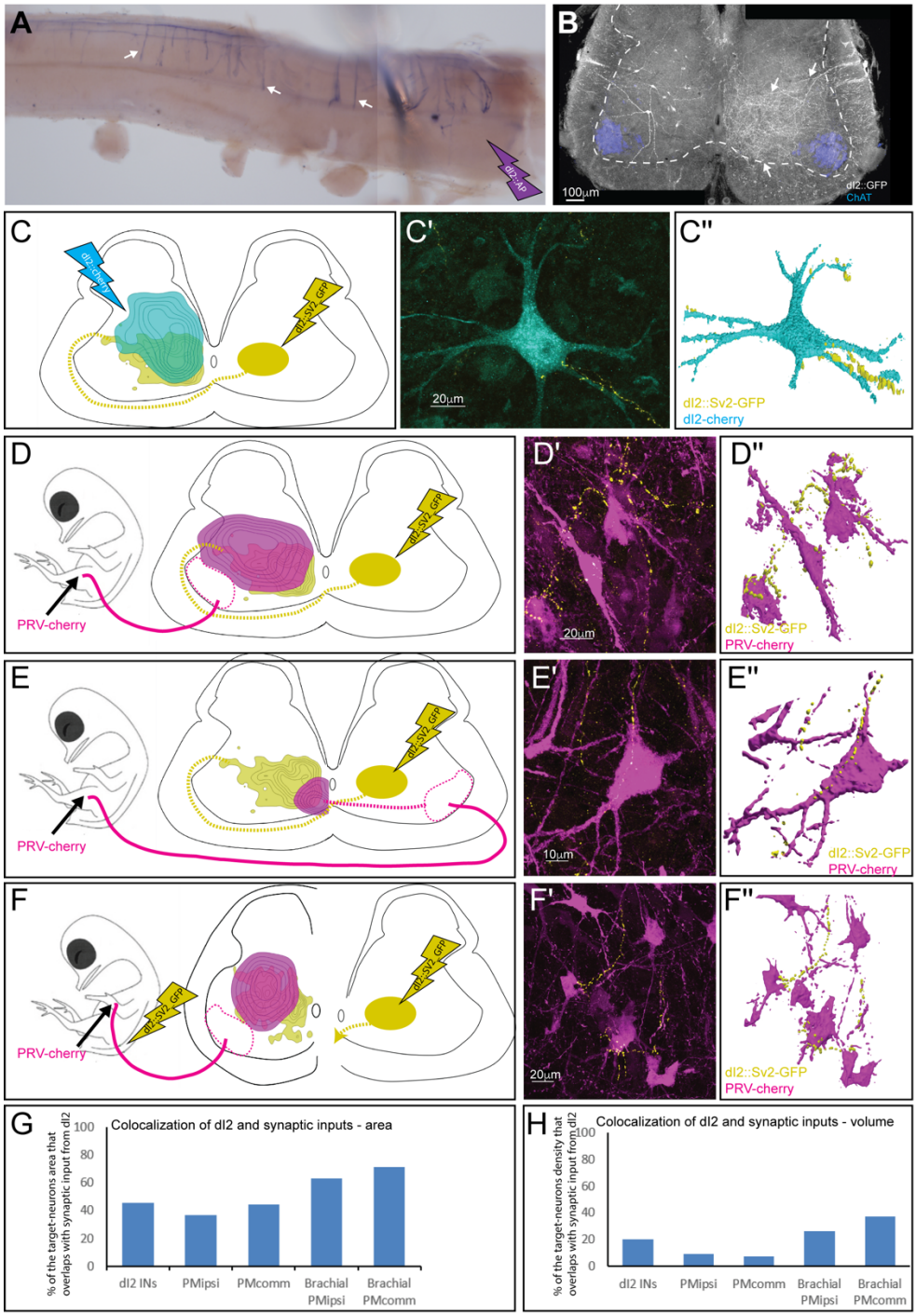

254

Figure 4: Spinal synaptic targets of dI2 neurons.

A. A whole mount staining of spinal cord (thoracic segments) expressing alkaline phosphatase (AP) in dI2 neurons. The lumbar dI2 neurons (not included in the image) were labeled with AP. dI2 axon collaterals project and into the spinal cord (arrows).

B. Cross section of an E17 embryo at the crural plexus level of the lumbar cord. The axon collaterals (white arrow) penetrating the gray matter of the contralateral side are evident.

Schematic representations of the experimental design for labeling synapses (dI2::SV2-GFP, yellow) and potential targets (magenta) supplemented by cell soma density and dI2 synaptic densities are illustrated in C, D, E, and F. Examples of target neurons contacting synaptic boutons of dI2 neurons are shown in C', D', E', and F'; and their 3D reconstruction in C'', D'', E'', and F''. Genetic labeling was attained using dI2 enhancers (Fig. S1) electroporated at HH18. Pre-MNs were labeled by injection of PRV-cherry into the hindlimbs (D, E) or the forelimb (F) musculature, at E13. The embryos were incubated until pre-MNs infection (39 hours).

C. dI2 neurons innervate the contralateral dI2 neurons (*N*=4735 synapses and *N*=374 cells, respectively).

D. dI2 neurons innervate ipsilateral projecting premotoneurons at the sciatic plexus level (*N*=4735 synapses and *N*=936 cells, respectively).

E. dI2 neurons innervate contralateral projecting premotoneurons at the sciatic plexus level (*N*=4735 synapses and *N*=47 cells, respectively).

F. dI2 neurons innervate brachial ipsilateral projecting premotoneurons (*N*=2215 synapses and *N*=286 cells, respectively).

G. Quantification of the overlap area of different synaptic targets and dI2 synapse density plots, as the percentage of overlap between dI2 synapses and the target.

H. Quantification of the overlap in volume of the different synaptic targets and dI2 synapse density plots, as the percentage of overlap between the synaptic target and dI2 synapses. See Figure S7.

256 **Silencing of dI2 neurons impairs stability of bipedal stepping**

257 The synaptic input to dI2 and their targets, implicate them as relaying information about
258 motor activity to the contralateral spinal cord and the cerebellum. Thus, we hypothesized
259 that manipulation of their neuronal activity may affect the dynamic profile of stepping.
260 To study the physiological role of dI2 neurons, we silenced their activity using bilateral
261 targeting of the tetanus toxin (*TeTX)* gene, to lumbar dI2s. EGFP was co-targeted in a 2/1
262 TeTX/EGFP ratio. EGFP expression in dI2 neurons and non-electroporated chicks was used as
263 a control. In order to maximize the number of targeted dI2 neurons, we combined genetic
264 targeting with the *Foxd3* enhancer and spatial placement of the electrodes at the dorsal
265 lumbar spinal cord (Fig. S1A). Embryos were electroporated at E3. Upon hatching, chicks
266 were trained for targeted over-ground locomotion.

267 To test whether silencing of dI2 impairs post-hatching development and muscle
268 strength, at P8 the weight of the chicks was measured and the foot grip power evaluated
269 (see below). Gait parameters of 4 controls and 5 *TeTX* treated chicks were measured while
270 chicks were walking toward their imprinting trainer along a horizontal track (6-20 walking
271 sessions, 5-8 strides each, per chick). Following the experiments, chicks were scarified and
272 their spinal cords were removed and processed for immune-detection of the efficacy of the
273 electroporation (Supplementary table S1).

274 The weight of all chicks was comparable within the range of 144.7±12.1 gr (Supp.
275 Table S1). As a functional measure of foot grip, we tested the ability of the chicks to maintain
276 balance on a tilted meshed surface. *TeTX*-manipulated chicks and control chicks, maintained
277 balance on the titled surface up to 63–70^0, with no apparent statistically significant
278 differences (Supplementary Table S1, Supplementary statistics). Thus, manipulation of dI2
279 neuronal activity did not impair post-hatching development and muscle strength.

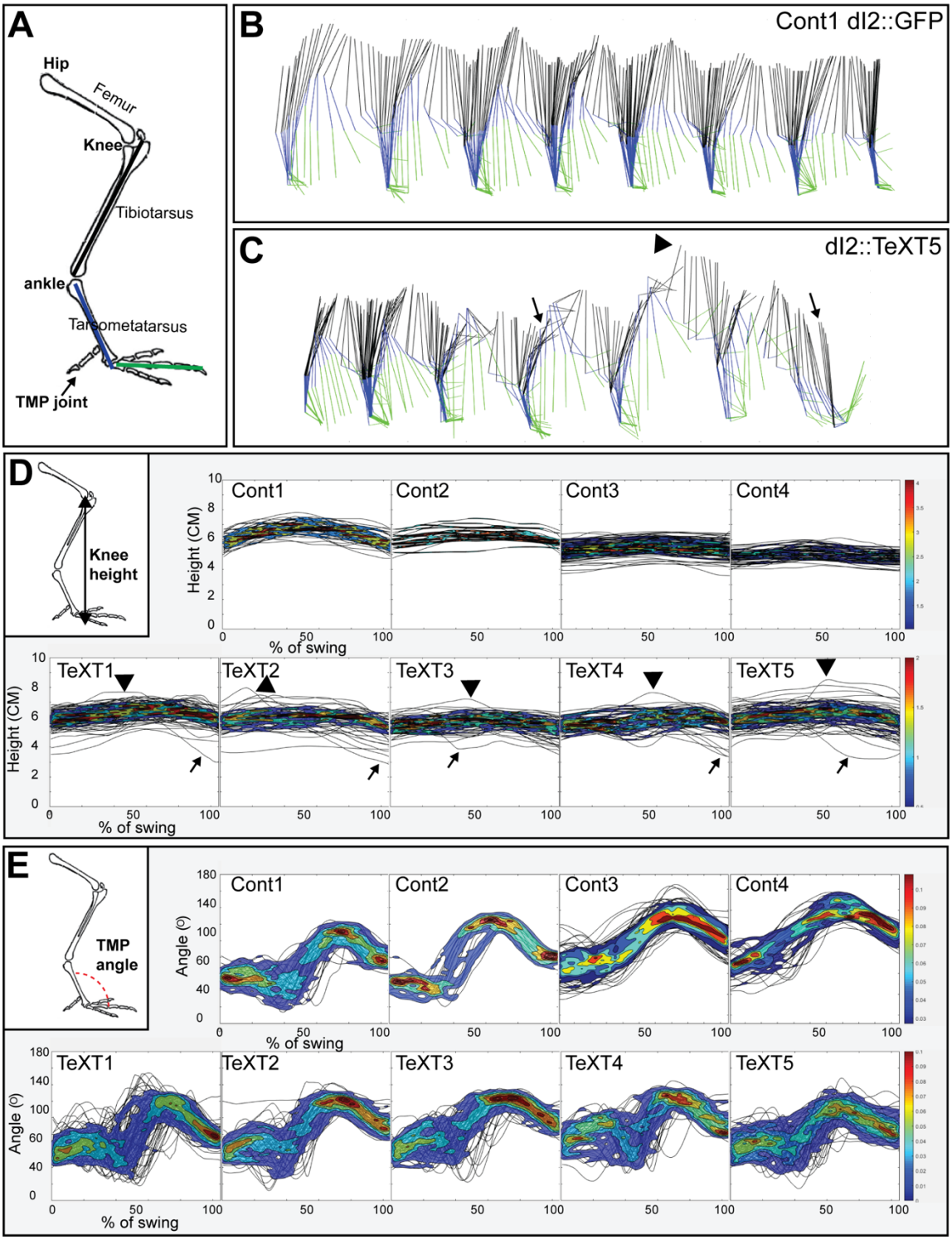

Figure 5: Kinematic analysis of locomotion in post-hatching chicks following neuronal silencing of dI2.

A. Schematic illustration of chick hindlimb joints (bold) and bones (regular). The knee joint connects between the femur and the tibiotarsus, the ankle connects the tibiotarsus and the tarsometatarsus which connects to the phalanges by the tarsometatarso-phalangeal joint (TMP). During the swing phase of birds, the ankle flexion leads to foot elevation, while the knee is relatively stable.

B,C. Stick diagrams of stepping in a control chicken d2::GFP (B) and in a d2::TeTX chicken (C). Arrows indicate falls and overshoots are denoted by arrowheads.

D. Overlays of knee height (demonstrated in insert) trajectories during the swing phase in all analyzed steps of each of the control and *TeTX* treated P8 hatchlings are shown superimposed with the respective 20%–80% color coded density plots as a function of the percentage of swing (see Text and Materials and Methods). Arrows indicate falls and overshoots are indicated by arrowheads.

E. Overlay of angular trajectories of the TMP joint (demonstrated in insert) during the swing phase in all analyzed strides of each of the control and *TeTX* treated P8 hatchlings are shown superimposed with the respective 20%–80% color coded density plots as a function of the percentage of swing (see Text and Materials and Methods).

282 Analysis of over ground locomotion of the control and *TeTX* treated chicks revealed
283 no significant differences is swing velocity and striding pattern. An 180^0 out-of-phase pattern
284 was found during stepping in all the manipulated and the control chicks (Fig. S8A, table 1,
285 Supplementary statistics). However, substantial differences were scored in stability
286 parameters: *TeTX* chicks exhibited whole-body collapses during stepping (Fig. 5B,C, Fig. 6A),
287 wide-base stepping (table 2), and variable limb movements (Fig.5 D,E, Fig. 6B,C, Fig. S8B,C
288 ,tables 3, Supplementary statistics).

289 Whole-body collapses: A collapse was scored as a decline of the knee height below 85% of
290 the average knee height at the stance phase of the step (arrow in Fig. 5C). Collapses were
291 usually followed by over-extensions (arrow head in Fig. 5C). We measured the number of
292 collapses in 50–190 steps. In control chicks, collapses occurred in 0.53±0.92% of the steps. In
293 *TeTX* manipulated chicks we observed collapses in 19.46±8.3% of the steps, significantly
294 different from the controls (Fig. 6A, Supplementary statistics). The collapses and over-
295 extensions were also manifested in the profiles of the knee height trajectory during the
296 swing phase (Fig. 5D).

297 Wide base stepping: Wide-base stance is typical of an unbalanced ataxic gait. The stride
298 width was measured between the two feet during the double stance phase of stepping. The
299 mean stride in *TeTX*-manipulated chicks 1,2,4, and 5 was significantly wider than the control
300 chicks, while the width in *TeXT3* was similar to the controls (Table 2, Supplementary
301 statistics).

302 Variable limb movements: In stable gait, limb trajectories are consistent from stride to
303 stride. For point by point comparisons of the trajectories in knee height and angles of the
304 TMP joint during the swing phase of stepping in control and TeTx manipulated chicks, the

305 swing phase was normalized using 126 consecutive epochs, and the data were displayed as a
306 function of the percentage of swing. Plots of the knee height and TMP angle trajectories
307 during the normalized swing in all the analyzed steps of each chick are shown superimposed
308 in Fig. 5D and Fig. 5E, respectively. These data demonstrate that the range of changes in
309 *TeTX*-manipulated chicks was higher comparing to control chicks.

310 Further analyses revealed that overall the control group shows lower Knee-height
311 and TMP angle ranges than the TeXT-treated group, even though there are differences
312 within groups (Fig. S8B,C). The average knee height range of the combined control chicks
313 (1.981±0.33) is significantly lower than the range of the combined TeXT treated chicks
314 (3.109±0.74) (Fig. 6B, Supplementary statistics). Similar comparison of the combined ranges
315 of angular excursions of the TMP joint during the normalized swing revealed that the
316 average angle of the controls group (49.34±16.03) is significantly lower than the average of
317 the TeXT-treated chicks (77±22.149). (Fig. 6C, Supplementary statistics).

318 Since the increased range of changes could be due to the effects of the substantial
319 increase in body collapses during stepping (Fig. 6A, see also Fig. 5), we excluded steps
320 featuring whole body collapses and reanalyzed the data. The data summarized in table 3,
321 shows that the significant difference between controls and the *TeXT*-treated chicks in the
322 range of the knee height and the TMP angle excursions was maintained. Thus, the increase
323 in irregularity in the *TeXT*-treated chicks is not only due to the body collapses of the *TeXT*-
324 treated chicks. Overall, the kinematic parameters of the *dI2-TeXT-treated* chicks
325 demonstrate a reduction in stability during locomotion, featuring a possible role of dI2 in
326 stabilizing bipedal stepping.

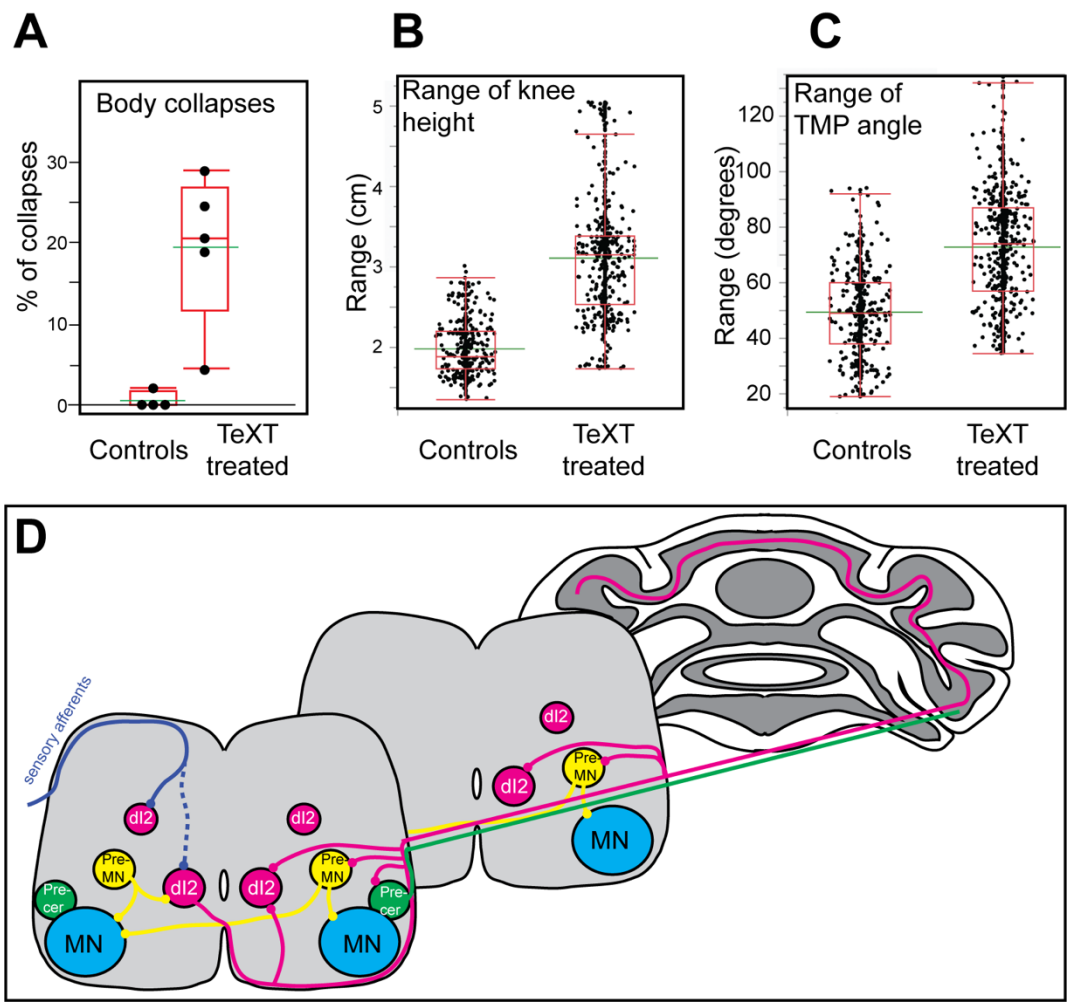

327

328 Figure 6. Increased inter-stride variability in TMP angle and knee height in *TeTX*-treated chicks.
A. The percentage of steps with body collapses in the controls and *TeTX* manipulated hatchlings (n=4 and n=5, respectively). p-value<0.0001 (Z-test). See table 3 for single chick fall proportions.
B. Analysis of the mean range of knee height changes during the swing phase of control and TeTX treated chicks (n=4 and n=5, respectively). p-value<0.0001 using a T-test allowing different variances.
See Figure S8B and table 3 for single chick data and statistical analysis details.
C. Analysis of the mean range of TMP angular excursions during the swing phase of control- and TeTX-treated chicks. (n=4 and n=5, respectively). p-value<0.0001 Watson and Williams F test.
See Figure S8C and table 3 for single chick data and statistical analysis details.
D. Schematic illustration showing the connectome of lumbar dI2 neurons. dI2s (magenta) receive synaptic input from sensory afferents (solid blue line indicates massive synaptic input and dashed blue line indicates sparse innervation), Inhibitory and excitatory premotoneurons (yellow), and from the contralateral lumbar dI2. dI2s innervate the contralateral lumbar and brachial premotoneurons (both commissural and ipsilateral projecting premotoneurons are innervated by dI2), the lumbar and brachial contralateral dI2, lumbar pre-cerebellar neurons (green) and the granule neurons in the cerebellum.

329 Table 1: Stride velocity and left-right phase in control and TeTx manipulated chicks

330 Swing velocity and left-right phase were measured and calculated as described in the

331 Materials and Methods. The Watson and Williams F test of the phase data (circular ANOVA)

332 were not statistically significant (See also Supplementary statistics).

333

chick	Ave. Swing velocity (cm/sec)	Mean left-right phase (°)	# of steps
TeTX1	46.78 ± 22.13	184.679 ± 33.003	113
TeTX2	62.24 ± 20.17	182.293 ± 32.01	63
TeTX3	48.06 ± 20.04	180.784 ± 31.064	69
TeTX4	57.24 ± 24.35	180.502 ± 36.291	59
TeTX5	36.66 ± 17.61	181.97 ± 35.787	93
Control 1 (GFP)	79.65 ± 37.77	182.369 ± 35.366	47
Control 2 (GFP)	41.91± 20.41	182.384 ± 26.708	19
Control3 (Not electroporated)	41.09± 16.59	N.D.	121
Control4 (Not electroporated)	42.3± 30.91	N.D.	51

334

335 Table 2: Maximum stride width in control and TeTx manipulated chicks

336 Stride width was measured as described in Materials and Methods. One-way ANOVA

337 followed by Dunnett's.

338

chick	maximum stride width (cm)	# of steps
TeTX1	5.11 ± 1.89	97
TeTX2	5.32 ± 1.38	36
TeTX3	4.5 ± 1.01	27
TeTX4	4.9 ± 1.16	49
TeTX5	5.82 ± 1.71	110
Control 8	4.15 ± 1.07	137
Control 9	4.32 ± 1.32	115

339

340 Table 3: Collapses, knee height and TMP angle ranges in control and TeTx manipulated

341 chicks.

342 Analysis of the range between the highest and lowest point of knee height and the highest

343 and lowest angle of the TMP joint in all steps before and after subtraction of collapsed steps.

344 When combined – the difference is statically significant (p-value<0.0001 for both metrics,

345 using a T-test allowing different variances).

346

chick	% of steps with collapse	TMP angle. Mean range(°)				# of steps				% of steps with collapse
		All steps Ave	Combined Ave	Minus collapses Ave	Minus collapses combined Ave	All steps Ave	Combined Ave	Minus collapses	Minus collapses combined Ave	
TeTX1	4.4	3.05 ± 0.49	3.11±0.74	2.87±0.38	2.83±0.57	82.27 ± 22	72.71±20.52	79.4±24.5	68.97±21.47	113
TeTX2	20.60	3.5 ± 0.3		3.35±0.47		71.79 ± 25		71.1±25.68		63
TeTX3	18.8	2.57 ± 0.31		2.27±0.26		64.17 ± 21		62.79±20.9		69
TeTX4	20.45	2.54 ± 0.55		2.477±0.56		72.48 ± 17		66.22±19.1		59
TeTX5	29	3.86 ± 0.83		3.2±0.2		72.86 ± 12		65.85±13.13		93
Control 1 (GFP)	2.12	1.91 ± 0.22	1.98±0.33	1.91±0.22	1.98±0.33	56.8 ± 16.4	49.34±16.03	56.95±16.6	49.4±16.18	47
Control 2 (GFP)	0	1.83 ± 0.25		1.83±0.25		41.42 ± 18.4		41.42 ± 18.4		19
Control3 (Not electroporated)	0	2.42 ± 0.23		2.42± 0.23		54.86 ± 9.65		54.86± 9.65		121
Control4 (Not electroporated)	0	1.75 ± 0.1		1.75± 0.1		44.12 ± 12.51		44.12± 12.51		51

347

348 **Discussion**

349 The VSCT is thought to provide peripheral and intrinsic spinal information to the cerebellum
350 in order to shape and update the output of spinal networks that execute motor behavior.
351 The lack of genetic accessibility to VSCT neurons hampers elucidation of their role in
352 locomotion. Using genetic toolbox to dissect the circuitry and manipulate neuronal activity
353 in the chick spinal cord, we studied spinal interneurons with VSCT characteristics. The main
354 findings in our study are that dI2 neurons in the chick lumbar spinal cord are commissural
355 neurons that innervate premotor neurons at the contralateral lumbar and brachial spinal
356 levels and granule neurons in the ipsilateral cerebellum. Hence, subpopulation of dI2 form a
357 part of the avian VSCT. Targeted silencing of dI2 neurons leads to impaired stepping in P8
358 hatchlings. We described the spatial distribution of sub-populations of dI2 neurons,
359 deciphered their connectomes, mapped the trajectory of their projection to the cerebellum,
360 and suggested possible mechanisms for the perturbed gait resulting from their genetic
361 silencing, as discussed below.

362 Using the intersection between genetic drivers and spatially restricted delivery of
363 reporters to define lumbar and brachial neurons, we have identified several targets of dI2
364 lumbar neurons. Ipsilateral lumbar dI2 neurons innervate contralateral lumbar dI2 neurons
365 as well as commissural and non-commissural lumbar pre-motoneurons. This connectivity
366 may affect the bilateral spinal output circuitry at the lumbar cord (e.g. (Bras et al., 1988,
367 Jankowska and Hammar, 2013)). Moreover, the ascending axons of lumbar dI2s, give off
368 grey matter collaterals innervating contralateral dI2s and commissural and non-commissural
369 pre-motoneurons throughout the brachial spinal cord (Fig. 6D). Therefore, lumbar dI2
370 neurons may also contribute to the inter-enlargement coupling described between the limb

371 and wing moving segments of the spinal cord (e.g. (Valenzuela et al., 1990, Ruder et al.,
372 2016) for forelimb to hindlimb coupling connectivity in mice).

373 We demonstrated that lumbar dI2s receive sensory innervation, pre-motor inhibitory
374 and excitatory innervation, and innervation from contralateral lumbar dI2s (Fig. 6D). Thus,
375 lumbar dI2 neurons can provide the cerebellum and contralateral premotor neurons with
376 proprioceptive information, copies of motor commands delivered from the ipsilateral pre-
377 motoneurons, and integrated information from contralateral dI2 neurons (Fig. 6D).

378 The unclear genetic origin of physiologically equivalent lumbar VSCT neurons,
379 prevented better understanding of their role in hindlimb locomotion. Our wiring and
380 neuronal-silencing studies implicated dI2 as a significant contributor to the regularity and
381 stability of locomotion in P8 hatchlings. The kinematic analysis of TeTX treated hatchlings,
382 revealed imbalanced locomotion with occasional collapses, increased stride variability, wide
383 base stepping, and variable limb movements during stepping.

384 The mechanisms accounting for the impaired stepping following dI2 silencing are still
385 unknown. One of the possible mechanisms is that silencing the dI2s perturbs the delivery of
386 peripheral and intrinsic feedback to the cerebellum, leading to unreliable updating of the
387 motor output produced by the locomotor networks, thereby impairing the bipedal stepping.
388 Another possible mechanism is based on the similarity of the gait instabilities of TeTX
389 treated hatchlings to ataxic motor disorders. Mammalian VSCT neurons receive descending
390 input from reticulospinal, rubrospinal and vestibulospinal pathways (Bras et al., 1988,
391 Jankowska and Hammar, 2013). Neurons from the lateral vestibular nucleus, have been
392 reported to innervate extensor motoneurons at the lumbar level, as well as interneurons
393 residing at the medial lamina VII (Murray et al., 2018), exactly at the location where dI2
394 neurons were found to reside in our study. Thus, the vestibulospinal tract may convey input

395 directly to the ipsilateral motoneurons, and indirectly to contralateral motoneurons through
396 dI2 neurons that innervate contralateral pre-motoneurons. This way silencing of dI2 neurons
397 is expected to interfere with the descending regulation of the stability of the bipedal gait.
398 The local spinal connections between dI2 and the contralateral premotor neurons
399 and contralateral dI2, may serve an important component of coordinated limb movements.
400 dI2 synapses were found on both ipsilateral and contralaterally projecting pre-
401 motorneurons, in their segmental level and in the brachial level, which regulates the
402 movement of the wings. Thus, dI2 neurons may affect the motor output of the contralateral
403 side of the cord, and also the ipsilateral side by contacting commissural pre-motorneurons.
404 In summary, our mapping studies of dI2 neurons and their connectomes followed by
405 characterization of the effects of their silencing on bipedal stepping, offer new insights on
406 the function of dI2 neurons in vertebrates. We suggest that lumbar dI2 neurons are not
407 merely used to relay sensory and intrinsic spinal networks information to the cerebellum,
408 but also act as active mediators of motor functions at the lumbar segments and at the wing
409 controlling brachial segments of the spinal cord. Further circuit deciphering studies of the
410 constituents of sub-populations of dI2s, their targets, and their descending inputs are
411 required to extend our understanding of the function of dI2 subpopulations in motor control
412 of movements.
413

414 **Materials and Methods**

415
416 **Animals**

417 Fertilized White Leghorn chicken eggs (Gil-Guy Farm, Israel) were incubated in standard
418 conditions at 38 °C. All experiments involved with animals were conducted in accordance
419 with the designated Experiments in Animals Ethic Committee policies and under its approval.

420
421 **3D reconstruction and density plots analysis**

422 The codes for both 3D reconstruction and the density plots analysis were written in Matlab.
423 The density plots were generated based on cross section images transformed to a standard
424 form. The background was subtracted, and the cells were filtered automatically based on
425 their soma area or using a manual approach. Subsequently, two-dimensional kernel density
426 estimation was obtained using the MATLAB function "*kde2d*". Finally, unless indicated
427 otherwise, a contour plot was drawn for density values between 20% and 80% of the
428 estimated density range, in six contour lines.

429
430 ***In-ovo* electroporation**

431 A DNA solution of 5 mg/mL was injected into the lumen of the neural tube at HH stage 17–
432 18 (E2.75-E3). Electroporation was performed using 3 × 50 ms pulses at 25–30 V, applied
433 across the embryo using a 0.5-mm tungsten wire and a BTX electroporator (ECM 830).
434 Following electroporation, 150–300 µL of antibiotic solution, containing 100 unit/mL
435 penicillin in Hank's Balanced Salt Solution (Biological Industry, Beit-Haemek) was added on
436 top of the embryos. Embryos were incubated for 3–19 days prior to further treatment or
437 analysis.

438
439 **Immunohistochemistry and *In situ* hybridization**

440 Embryos were fixed overnight at 4°C in 4% paraformaldehyde/0.1 M phosphate buffer,
441 washed twice with phosphate buffered saline (PBS), incubated in 30% sucrose/PBS for 24 h,
442 and embedded in OCT (Scigen, Grandad, USA). Cryostat sections (20 µm). Sections were
443 collected on Superfrost Plus slides and kept at −20°C. For 100-µm sections, spinal cords were
444 isolated from the fixed embryos and subsequently embedded in warm 5% agar (in PBS), and
445 100µm sections (E12–E17) were cut with a Vibratome. Sections were collected in wells (free-
446 floating technique) and processed for immunolabeling.
447 The following primary antibodies were used—rabbit polyclonal GFP antibody 1:1000
448 (Molecular Probes, Eugene, Oregon, USA), mouse anti-GFP 1:100, Goat anti-GFP 1:300
449 (ABcam), rabbit anti-RFP 1:1000 (Acris), goat ChAT antibody 1:300 (Cemicon, Temecula, CA,
450 USA), mouse anti-synaptotagmin antibody 1:100 (ASV30), mouse anti-Lhx1/5 1:100 (4F2),
451 mouse anti-FoxP4 1:50 (hybridoma bank, University of Iowa, Iowa City, USA), mouse anti
452 Brn3a 1:50 (Mercury), rabbit anti-Pax2 antibody 1:50 (ABcam), chicken anti-lacZ antibody
453 1:300 (ABcam), rabbit anti Clabindin 1:200 (Swant), rabbit VGUT2 antibody (Synaptic
454 Systems, Göttingen, Germany), goat anti FoxP2 1:1000 (ABcam), goat anti FoxP1 1:100 (R&D
455 Systems) and rabbit anti 5HT 1:100 (Immunostar). The following secondary antibodies were
456 used: Alexa Fluor 488/647-AffiniPure Donkey Anti mouse, rabbit and goat (Jackson) and
457 Rhodamin Red-X Donkey Anti mouse and rabbit (Jackson). Images were taken under a
458 microscope (Eclipse Ni; Nikon) with a digital camera (Zyla sCMOS; Andor) or a confocal
459 microscope (FV1000; Olympus).
460 *In situ* hybridization was performed as described (Avraham O et al., 2010). The following
461 probes were employed: Foxd3, vGlut2 and GAD1 probes were amplified from a cDNA of E6
462 chick embryo using the following primers. Foxd3: forward-TCATCACCATGGCCATCCTG and
463 Reverse -GCTGGGCTCGGATTTCACGAT. vGlut2: forward -GGAAGATGGGAAGCCCATGG and

464 Reverse -GAAGTCGGCAATTTGTCCCC. GAD1: forward-TCTCACCTGGAGGAGCCATC and
465 Reverse -CCTGAGGCTGATATCCAACC. T7 RNApol cis-binding sequence was added to the
466 reverse primers.
467
468 **AP staining**
469 The treated embryos were fixed with 4% paraformaldehyde–PBS for 24 h at 4°C, and washed
470 twice with PBS for 30 min at 4°C. The fixed embryos were incubated at 65°C in PBS for 8 to
471 16 h to inactivate the endogenous AP activity. The treated embryos were washed with 100
472 mM Tris–Cl (pH 9.5) containing 100 mM NaCl and 50 mM MgCl2, and the residual Placental
473 alkaline phosphatase activity was visualized by incubating the embryos with NBT/BCIP
474 (Roche) in the same buffer at 4°C for 24 h. After extensively washing the embryos with PBS–
475 5 mM EDTA, the spinal cord was imaged.
476
477 **Analysis of Left-right phase**
478 Stride duration was measured as the time from 'Right toe-off'/foot-off' to the next Right
479 'toe-off' (as a complete stride cycle for the right leg), and the 'half-cycle' duration as the
480 time of Right-toe off to the time of Left toe off. the following formula was used to calculate
481 the phase: ((LeftToeOff_1 - RightToeOff_1)/ (RightToeOff_2 – RightToeOff_1))*360.
482
483 **PRV infection**
484 We used two isogenic recombinants of an attenuated PRV strain Bartha (PRV Bartha) that
485 express enhanced GFP (PRV152) and monomeric red fluorescent protein (PRV614). The
486 viruses were harvested from Vero cell cultures at titers 4 × 108, 7 × 108 and 1 × 109 plaque
487 forming units (pfu/mL), respectively. Viral stocks were stored at −80°C. Injections of 3 µL of
488 PRV152 or PRV614 were made into the thigh musculature of E13 or E14 chick embryos, using

489 Hamilton syringe (Hamilton; Reno, NV, USA) equipped with a 33-gauge needle. The embryos
490 were incubated for 36–40 h and sacrificed for analysis. For spinocerebellar projecting
491 neurons labeling, we used a replication defective HSV (TK^-) that contains a lacZ reporter. The
492 virus was injected *in ovo* into the cerebellum of E12-15 embryos, and the embryos were
493 further incubated for 40–48. Alternatively, cholera toxin subunit B (CTB) conjugated to Alexa
494 Fluor™ 647 (ThermoFisher) was used for the same purpose, and was injected to the
495 cerebellum of E12–15 embryos together with the virus for visualization of both cerebellar
496 projecting neurons and upstream neurons.
497
498 **Force test**
499 The muscle strength was evaluated using the measurement of the angle of the fall from a
500 ladder with a gradually increasing-angle. This test was repeated for each chicken at least 3
501 times, and the average falling angle was calculated.
502
503 **Behavioral tests and analysis**
504 The embryos were bilaterally electroporated, and were then allowed let to develop and
505 hatch in a properly humidified and heated incubator. Afterwards, within 32 hours post
506 hatching, the hatchling chicks were imprinted on the trainer. The P8 chicks were filmed in
507 slow motion (240 fps) freely walking (side and top views). The following parameters were
508 scored: 1) weight, 2) foot grip power, 3) kinematics parameters during overground
509 locomotion: a) swing velocity, b) swing and stance duration, c) phase of footfalls, d) height of
510 knee and tarsometatarso-phalangeal (TMP) joints, e) angles of the TMP and ankle joints, and
511 f) stride width (distance between feet during the double stance phase).
512 Using a semi-automated Matlab-based tracking software (Hedrick, 2008), several
513 points of interest were encoded. The leg joints as well as the eye and the tail were tracked.

514 The position of these reference points was used for computational analysis using an in-
515 house Matlab code for calculating different basic locomotion parameters (e.g. stick
516 diagrams, velocity, joints trajectory, angles, range, and elevation), steps pattern, and degree
517 of similarity (Haimson B et al. *in preparation*). Dunnett's test (Dunnett, 1955) was used to
518 perform multiple comparisons of group means following One-way ANOVA. Circular statistics
519 was used for analyses of angular data. Circular statistics was used for analyses of angular
520 data, utilizing Oriana (KCS, version 4).

Acknowledgements: The authors thank Haya Falk for PRV purification; Alona Katzir, Cole Bendor, Mevaseret Avital, Sapir Shevah, Eitan Yisraeli, Ruth Segal, Fedaa Bazan and Eden Kimchi for technical assistance; Michael O'Donovan for comments on the manuscript. This work was supported by grants to AK from the Israel Science Foundation (grant No. 1400/16), The US-Israel Binational Science Foundation (grant No. 2017/172) and the Avraham and Ida Baruch endowment fund.

Author contributions:

B.H., A.Klar and ALT designed research; B.H., and Y.H. preformed research; B.H., and M.D. generated the kinematic analysis tools; Y.C. assisted in the post hatching analysis; A. Kania provided reagents and comments on the research; B.H., A.Klar and ALT analyzed the data; B.H., A.Klar and ALT wrote the paper.

Competing interests:

The authors declare no competing of interest.

538 **References**

539 ALAYNICK, W. A., JESSELL, T. M. & PFAFF, S. L. 2011. SnapShot: spinal cord
540 development. *Cell,* 146**,** 178-178 e1.
541 ANDERSSON, L. S., LARHAMMAR, M., MEMIC, F., WOOTZ, H., SCHWOCHOW, D.,
542 RUBIN, C.-J., PATRA, K., ARNASON, T., WELLBRING, L., HJALM, G.,
543 IMSLAND, F., PETERSEN, J. L., MCCUE, M. E., MICKELSON, J. R., COTHRAN,
544 G., AHITUV, N., ROEPSTORFF, L., MIKKO, S., VALLSTEDT, A., LINDGREN,
545 G., ANDERSSON, L. & KULLANDER, K. 2012. Mutations in DMRT3 affect
546 locomotion in horses and spinal circuit function in mice. *Nature,* 488**,** 642-6.
547 AVRAHAM, O., HADAS, Y., VALD, L., ZISMAN, S., SCHEJTER, A., VISEL, A. &
548 KLAR, A. 2009. Transcriptional control of axonal guidance and sorting in dorsal
549 interneurons by the Lim-HD proteins Lhx9 and Lhx1. *Neural Dev,* 4**,** 21.
550 BERMINGHAM, N. A., HASSAN, B. A., WANG, V. Y., FERNANDEZ, M., BANFI, S.,
551 BELLEN, H. J., FRITZSCH, B. & ZOGHBI, H. Y. 2001. Proprioceptor pathway
552 development is dependent on Math1. *Neuron,* 30**,** 411-22.
553 BIKOFF, J. B., GABITTO, M. I., RIVARD, A. F., DROBAC, E., MACHADO, T. A., MIRI,
554 A., BRENNER-MORTON, S., FAMOJURE, E., DIAZ, C., ALVAREZ, F. J.,
555 MENTIS, G. Z. & JESSELL, T. M. 2016. Spinal Inhibitory Interneuron Diversity
556 Delineates Variant Motor Microcircuits. *Cell,* 165**,** 207-219.
557 BRAS, H., CAVALLARI, P. & JANKOWSKA, E. 1988. Demonstration of initial axon
558 collaterals of cells of origin of the ventral spinocerebellar tract in the cat. *J Comp*
559 *Neurol,* 273**,** 584-92.
560 BUI, T. V., AKAY, T., LOUBANI, O., HNASKO, T. S., JESSELL, T. M. &
561 BROWNSTONE, R. M. 2013. Circuits for grasping: spinal dI3 interneurons mediate
562 cutaneous control of motor behavior. *NEURON,* 78**,** 191-204.
563 CHENG, L., ARATA, A., MIZUGUCHI, R., QIAN, Y., KARUNARATNE, A., GRAY, P.
564 A., ARATA, S., SHIRASAWA, S., BOUCHARD, M., LUO, P., CHEN, C. L.,
565 BUSSLINGER, M., GOULDING, M., ONIMARU, H. & MA, Q. 2004. Tlx3 and
566 Tlx1 are post-mitotic selector genes determining glutamatergic over GABAergic cell
567 fates. *Nat Neurosci,* 7**,** 510-7.
568 DELILE, J., RAYON, T., MELCHIONDA, M., EDWARDS, A., BRISCOE, J. & SAGNER,
569 A. 2019. Single cell transcriptomics reveals spatial and temporal dynamics of gene
570 expression in the developing mouse spinal cord. *Development,* 146.
571 DUNNETT, C. W. 1955. A Multiple Comparison Procedure for Comparing Several
572 Treatments with a Control. *Journal of the American Statistical Association,* 50**,** 1096-
573 1121.
574 FRANCIUS, C., HARRIS, A., RUCCHIN, V., HENDRICKS, T. J., STAM, F. J., BARBER,
575 M., KUREK, D., GROSVELD, F. G., PIERANI, A., GOULDING, M. & CLOTMAN,
576 F. 2013. Identification of multiple subsets of ventral interneurons and differential
577 distribution along the rostrocaudal axis of the developing spinal cord. *PLoS One,* 8**,**
578 e70325.
579 FURUE, M., UCHIDA, S., SHINOZAKI, A., IMAGAWA, T., HOSAKA, Y. Z. &
580 UEHARA, M. 2010. Spinocerebellar projections from the cervical and lumbosacral
581 enlargements in the chicken spinal cord. *Brain Behav Evol,* 76**,** 271-8.
582 FURUE, M., UCHIDA, S., SHINOZAKI, A., IMAGAWA, T., HOSAKA, Y. Z. &
583 UEHARA, M. 2011. Trajectories in the spinal cord and the mediolateral spread in the
584 cerebellar cortex of spinocerebellar fibers from the unilateral lumbosacral enlargement
585 in the chicken. *Brain Behav Evol,* 77**,** 45-54.
586 GOSGNACH, S., LANUZA, G. M., BUTT, S. J., SAUERESSIG, H., ZHANG, Y.,
587 VELASQUEZ, T., RIETHMACHER, D., CALLAWAY, E. M., KIEHN, O. &

588 GOULDING, M. 2006. V1 spinal neurons regulate the speed of vertebrate locomotor
589 outputs. *Nature,* 440**,** 215-9.
590 GRIENER, A., ZHANG, W., KAO, H., WAGNER, C. & GOSGNACH, S. 2015. Probing
591 diversity within subpopulations of locomotor-related V0 interneurons. *Dev Neurobiol,*
592 75**,** 1189-203.
593 HADAS, Y., ETLIN, A., FALK, H., AVRAHAM, O., KOBILER, O., PANET, A., LEV-
594 TOV, A. & KLAR, A. 2014. A 'tool box' for deciphering neuronal circuits in the
595 developing chick spinal cord. *Nucleic Acids Res,* 42**,** e148.
596 HANTMAN, A. W. & JESSELL, T. M. 2010. Clarke's column neurons as the focus of a
597 corticospinal corollary circuit. *Nat Neurosci,* 13**,** 1233-9.
598 HEDRICK, T. L. 2008. Software techniques for two- and three-dimensional kinematic
599 measurements of biological and biomimetic systems. *Bioinspir Biomim,* 3**,** 034001.
600 JANKOWSKA, E. & HAMMAR, I. 2013. Interactions between spinal interneurons and
601 ventral spinocerebellar tract neurons. *J Physiol,* 591**,** 5445-51.
602 JESSELL, T. M. 2000. Neuronal specification in the spinal cord: inductive signals and
603 transcriptional codes. *Nat Rev Genet,* 1**,** 20-9.
604 JIANG, J., AZIM, E., EKEROT, C. F. & ALSTERMARK, B. 2015. Direct and indirect
605 spino-cerebellar pathways: shared ideas but different functions in motor control. *Front*
606 *Comput Neurosci,* 9**,** 75.
607 LAI, H. C., SEAL, R. P. & JOHNSON, J. E. 2016. Making sense out of spinal cord
608 somatosensory development. *Development,* 143**,** 3434-3448.
609 MORIKAWA, Y., HISAOKA, T. & SENBA, E. 2009. Characterization of Foxp2-expressing
610 cells in the developing spinal cord. *Neuroscience,* 162**,** 1150-62.
611 MURRAY, A. J., CROCE, K., BELTON, T., AKAY, T. & JESSELL, T. M. 2018. Balance
612 Control Mediated by Vestibular Circuits Directing Limb Extension or Antagonist
613 Muscle Co-activation. *Cell Rep,* 22**,** 1325-1338.
614 OSSEWARD, P. J., 2ND & PFAFF, S. L. 2019. Cell type and circuit modules in the spinal
615 cord. *Curr Opin Neurobiol,* 56**,** 175-184.
616 RUDER, L., TAKEOKA, A. & ARBER, S. 2016. Long-Distance Descending Spinal Neurons
617 Ensure Quadrupedal Locomotor Stability. *Neuron,* 92**,** 1063-1078.
618 SAKAI, N., INSOLERA, R., SILLITOE, R. V., SHI, S.-H. & KAPRIELIAN, Z. 2012. Axon
619 sorting within the spinal cord marginal zone via Robo-mediated inhibition of N-
620 cadherin controls spinocerebellar tract formation. *The Journal of neuroscience : the*
621 *official journal of the Society for Neuroscience,* 32**,** 15377-87.
622 SPANNE, A. & JORNTELL, H. 2013. Processing of multi-dimensional sensorimotor
623 information in the spinal and cerebellar neuronal circuitry: a new hypothesis. *PLoS*
624 *Comput Biol,* 9**,** e1002979.
625 STECINA, K., FEDIRCHUK, B. & HULTBORN, H. 2013. Information to cerebellum on
626 spinal motor networks mediated by the dorsal spinocerebellar tract. *J Physiol,* 591**,**
627 5433-43.
628 SWEENEY, L. B., BIKOFF, J. B., GABITTO, M. I., BRENNER-MORTON, S., BAEK, M.,
629 YANG, J. H., TABAK, E. G., DASEN, J. S., KINTNER, C. R. & JESSELL, T. M.
630 2018. Origin and Segmental Diversity of Spinal Inhibitory Interneurons. *Neuron,* 97**,**
631 341-355 e3.
632 UEHARA, M., AKITA, M., FURUE, M., SHINOZAKI, A. & HOSAKA, Y. Z. 2012.
633 Laterality of spinocerebellar neurons in the chicken spinal cord. *J Vet Med Sci,* 74**,**
634 495-8.
635 VALENZUELA, J. I., HASAN, S. J. & STEEVES, J. D. 1990. Stimulation of the brainstem
636 reticular formation evokes locomotor activity in embryonic chicken (in ovo). *Brain*
637 *Res Dev Brain Res,* 56**,** 13-8.

YUENGERT, R., HORI, K., KIBODEAUX, E. E., MCCLELLAN, J. X., MORALES, J. E., HUANG, T. P., NEUL, J. L. & LAI, H. C. 2015. Origin of a Non-Clarke's Column Division of the Dorsal Spinocerebellar Tract and the Role of Caudal Proprioceptive Neurons in Motor Function. *Cell Rep,* 13**,** 1258-1271.

644 **Figure legends**

645 Figure 1: Characterization and classification of dI2 neurons during embryonic development.
646 dI2 interneurons were labeled by genetic intersection between Foxd3 and Ngn1 enhancers
647 (Avraham et al., 2009) (See Figure S1).

648 **A–D.** dI2 axonal projection during development. At E5 (A) post mitotic dI2 neurons assume a
649 dorsolateral position and start to migrate ventrally. At E6 (B) dI2 neurons occupy the mid-
650 lateral domain. At E15-17 dI2 neurons are located at the medial lamina VII at the lumbar
651 level (LS3) (C) and the thoracic level (T1) (D). dI2 axons cross the floor plate (yellow
652 arrowheads), turn longitudinally at the ventral funiculus (white arrowheads) and eventually
653 elongate at the lateral funiculus (white arrows).

654 **E.** A graph indicating the fraction of dI2 neurons expressing TFs during development (based
655 on data from three E5, two E6 and two E14 embryos). **F.** Cross section of an E17 embryo at
656 the lumbar spinal cord (crural plexus level, LS2). Small-diameter dI2 neurons residing in
657 lamina VII (F') and ventromedial large-diameter dI2 neurons in lamina VIII (F"). **G.** Density
658 plots of dI2 somata in the sciatic plexus level (cyan, *N*=374 cells), $dI2_{large}$ (magenta) and
659 $dI2_{small}$ (yellow) INs (*N*=33 and *N*=344 cells, respectively, from 2 embryos).
660 See Figure S2 and S3.

661
662 Figure 2: dI2 neurons project to the cerebellum.

663 **A.** Experimental setup for labeling of cerebellar projecting dI2 neurons. dI2 neurons were
664 genetically targeted at HH18, and pre-cerebellar neurons were labeled using intra-cerebellar
665 injection of CTB or replication defective HSV-LacZ at E15. **B.** A cross section of E17 brainstem
666 and cerebellum. The dashed polygon in B' is magnified in B. dI2 axons reach the cerebellum,
667 enter into it via the superior cerebellar peduncle and cross the cerebellar midline. Calbindin

668 (Purkinje neurons, magenta (B') or red (B)), synaptotagmin (yellow). **C.** A cross section of E17
669 cerebellar cortex. Lumbar-originating dI2 synapses (cyan) in the granular layer of the
670 anterior cerebellar cortex. Calbindin (Purkinje neurons, magenta), synaptotagmin (yellow).
671 **D.** A cross section of an E15 embryo at the lumbar spinal cord level (sciatic plexus level). Pre-
672 cerebellar neurons were infected and labeled by HSV-LacZ (magenta), and dI2 neurons
673 express GFP (cyan). A large-diameter dI2 neuron co-expressing LacZ and GFP is indicated by
674 an arrow (magnification of the two channels in the insets). **E.** Density plots of dI2 and pre-
675 cerebellar neurons (density values 10-90%) in the sciatic plexus segments (*N*=374 and *N*=289
676 cells, respectively). **F.** CTB labeled pre-cerebellar neuron (magenta) is contacted by dI2
677 axonal terminals (cyan). **G.** Density plots of dI2 synapses and pre-cerebellar neuron somata
678 (density values 10-90%) in the sciatic plexus segments (*N*=4735 synapses and *N*=289 cells,
679 respectively). **H,I.** Quantification of the overlap in area and volume of the two density plots.
680 The plots are based on data from 3 embryos.
681 See Figure S4.
682
683 Figure 3: Synaptic inputs to dI2 neurons.
684 Schematic representations of the experimental design for labeling dI2::GFP or dI2::cherry INs
685 (cyan) and potential sources of synaptic inputs (yellow or magenta), supplemented by cell
686 soma density of dI2 INs and the synaptic densities are illustrated in A, B, C, D, E. The density
687 values presented are 10-80%, 20-80%, 25-80%, 30-50% and 20-80%, respectively.
688 Examples of dI2 neurons contacted by axons or synaptic boutons are shown in A', B', C', and
689 D'; and their 3D reconstruction in A'', B'', C'', and D''. Genetic labeling was attained using
690 specific enhancers (Fig. S1) electroporated at HH18.

691 **A.** DRG neurons form contacts on dI2 neurons. Inset in A: cross section of and E17 embryo at
692 the crural plexus level of the lumbar cord. A dorsally located dI2 neuron contacted by
693 numerous sensory afferents, magnified in A' and 3D-reconstructed in A''. (*N*=18 sections)
694 **B.** Premotoneurons form contacts on dI2 neurons. dI2 neurons were labeled at HH18. At
695 E13, PRV virus was injected to the leg musculature, and the embryo was incubated until
696 premotoneuronal infection (39 hours) (*N*=34 sections).
697 **C.** dI1 neurons form synapses on dI2 neurons. (*N*=8568 synapses). C': A representative
698 SV2::cherry synapse on dI2 dendrite, positive for synaptotagmin. Demonstrated by a
699 horizontal and vertical optical sections in Z-axis (see cursors and color channels).
700 **D.** V1 neurons form synapses on dI2 neurons. (*N*=1923 synapses).
701 **E.** dI2 neurons do not have 5HT synaptic terminals (*N*=1718 synapses). E17 cross sections of
702 dI2::GFP labeled embryos were stained for 5HT.
703 **F.** Quantification of the overlap area of the different input sources and dI2 neuron densities
704 plots.
705 See Figure S5, S6.
706
707 Figure 4: Spinal synaptic targets of dI2 neurons.
708 **A.** A whole mount staining of spinal cord (thoracic segments) expressing alkaline
709 phosphatase (AP) in dI2 neurons. The lumbar dI2 neurons (not included in the image) were
710 labeled with AP. dI2 axon collaterals project and into the spinal cord (arrows).
711 **B.** Cross section of an E17 embryo at the crural plexus level of the lumbar cord. The axon
712 collaterals (white arrow) penetrating the gray matter of the contralateral side are evident.
713 Schematic representations of the experimental design for labeling synapses (dI2::SV2-GFP,
714 yellow) and potential targets (magenta) supplemented by cell soma density and dI2 synaptic

715 densities are illustrated in C, D, E, and F. Examples of target neurons contacting synaptic
716 boutons of dI2 neurons are shown in C', D', E', and F'; and their 3D reconstruction in C'', D'',
717 E'', and F''. Genetic labeling was attained using dI2 enhancers (Fig. S1) electroporated at
718 HH18. Pre-MNs were labeled by injection of PRV-cherry into the hindlimbs (D, E) or the
719 forelimb (F) musculature, at E13. The embryos were incubated until pre-MNs infection (39
720 hours).
721 **C.** dI2 neurons innervate the contralateral dI2 neurons (*N*=4735 synapses and *N*=374 cells,
722 respectively).
723 **D.** dI2 neurons innervate ipsilateral projecting premotoneurons at the sciatic plexus level
724 (*N*=4735 synapses and *N*=936 cells, respectively).
725 **E.** dI2 neurons innervate contralateral projecting premotoneurons at the sciatic plexus level
726 (*N*=4735 synapses and *N*=47 cells, respectively).
727 **F.** dI2 neurons innervate brachial ipsilateral projecting premotoneurons (*N*=2215 synapses
728 and *N*=286 cells, respectively).
729 **G.** Quantification of the overlap area of different synaptic targets and dI2 synapse density
730 plots, as the percentage of overlap between dI2 synapses and the target.
731 **H.** Quantification of the overlap in volume of the different synaptic targets and dI2 synapse
732 density plots, as the percentage of overlap between the synaptic target and dI2 synapses.
733 See Figure S7.
734
735 Figure 5: Kinematic analysis of locomotion in post-hatching chicks following neuronal
736 silencing of dI2.
737 **A.** Schematic illustration of chick hindlimb joints (bold) and bones (regular). The knee joint
738 connects between the femur and the tibiotarsus, the ankle connects the tibiotarsus and the

739 tarsometatarsus which connects to the phalanges by the tarsometatarso-phalangeal joint
740 (TMP). During the swing phase of birds, the ankle flexion leads to foot elevation, while the
741 knee is relatively stable.
742 **B,C.** Stick diagrams of stepping in a control chicken d2::GFP (B) and in a d2::TeTX chicken (C).
743 Arrows indicate falls and overshoots are denoted by arrowheads.
744 **D.** Overlays of knee height (demonstrated in insert) trajectories during the swing phase in all
745 analyzed steps of each of the control and *TeTX* treated P8 hatchlings are shown
746 superimposed with the respective 20%–80% color coded density plots as a function of the
747 percentage of swing (see Text and Materials and Methods). Arrows indicate falls and
748 overshoots are indicated by arrowheads.
749 **E.** Overlay of angular trajectories of the TMP joint (demonstrated in insert) during the swing
750 phase in all analyzed strides of each of the control and *TeTX* treated P8 hatchlings are shown
751 superimposed with the respective 20%–80% color coded density plots as a function of the
752 percentage of swing (see Text and Materials and Methods).
753
754 Figure 6. Increased inter-stride variability in TMP angle and knee height in *TeTX*-treated
755 chicks.
756 **A.** The percentage of steps with body collapses in the controls and *TeTX* manipulated
757 hatchlings (n=4 and n=5, respectively). p-value<0.0001 (Z-test). See table 3 for single chick
758 fall proportions.
759 **B.** Analysis of the mean range of knee height changes during the swing phase of control and
760 TeTX treated chicks (n=4 and n=5, respectively). p-value<0.0001 using a T-test allowing
761 different variances.
762 See Figure S8B and table 3 for single chick data and statistical analysis details.

763 **C.** Analysis of the mean range of TMP angular excursions during the swing phase of control-

764 and TeTX-treated chicks. (n=4 and n=5, respectively).

765 p-value<0.0001 Watson and Williams F test.

766 See Figure S8C and table 3 for single chick data and statistical analysis details.

767 **D.** Schematic illustration showing the connectome of lumbar dI2 neurons. dI2s (magenta)

768 receive synaptic input from sensory afferents (solid blue line indicates massive synaptic

769 input and dashed blue line indicates sparse innervation), Inhibitory and excitatory

770 premotoneurons (yellow), and from the contralateral lumbar dI2. dI2s innervate the

771 contralateral lumbar and brachial premotoneurons (both commissural and ipsilateral

772 projecting premotoneurons are innervated by dI2), the lumbar and brachial contralateral

773 dI2, lumbar pre-cerebellar neurons (green) and the granule neurons in the cerebellum

Fig. 1

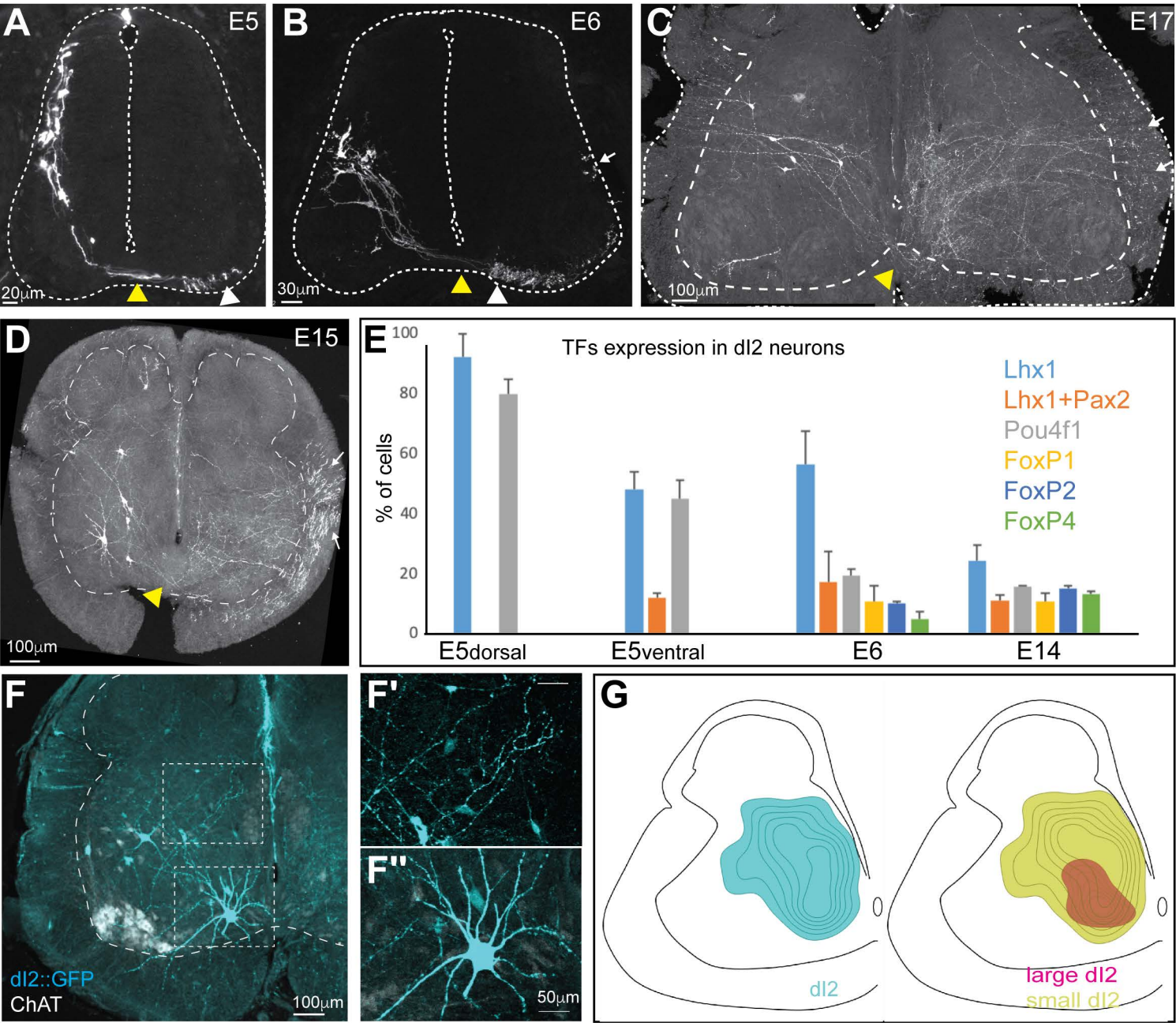
A
E5
20µm
B
E6
30µm
C
E17
100µm
D
E15
100µm
E
TFs expression in dI2 neurons
% of cells
100
80
60
40
20
0
Lhx1
Lhx1+Pax2
Pou4f1
FoxP1
FoxP2
FoxP4
E5dorsal
E5ventral
E6
E14
F
dI2::GFP
ChAT
100µm
F'
F''
50µm
G
dI2
large dI2
small dI2

Fig. 2

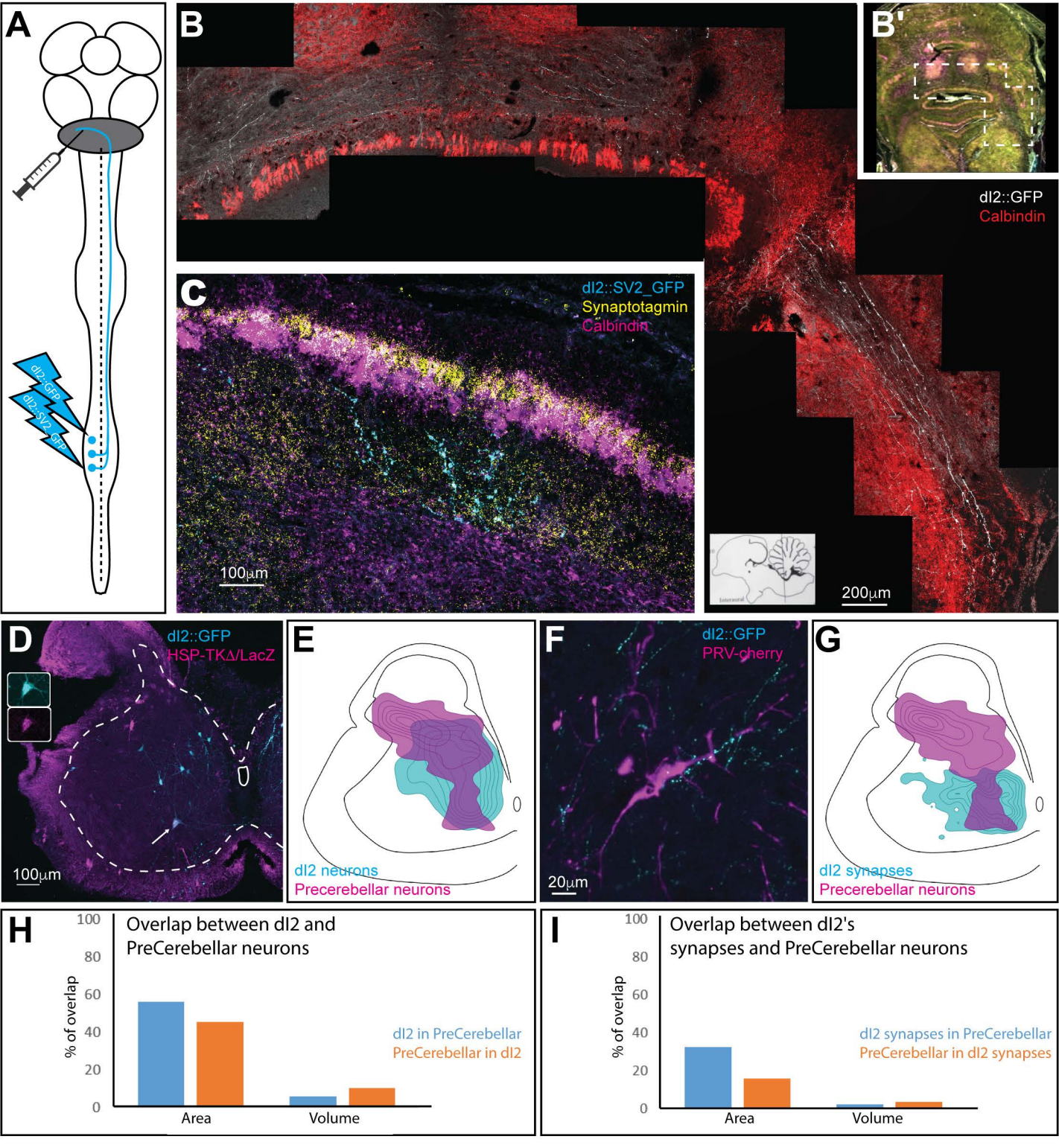
A
dI2::GFP
dI2::SV2_GFP
B
B'
dI2::GFP
Calbindin
200µm
C
dI2::SV2_GFP
Synaptotagmin
Calbindin
100µm
D
dI2::GFP
HSP-TKΔ/LacZ
100µm
E
dI2 neurons
Precerebellar neurons
F
dI2::GFP
PRV-cherry
20µm
G
dI2 synapses
Precerebellar neurons
H
Overlap between dI2 and PreCerebellar neurons
% of overlap
100
80
60
40
20
0
dI2 in PreCerebellar
PreCerebellar in dI2
Area
Volume
I
Overlap between dI2's synapses and PreCerebellar neurons
% of overlap
100
80
60
40
20
0
dI2 synapses in PreCerebellar
PreCerebellar in dI2 synapses
Area
Volume

Fig. 3

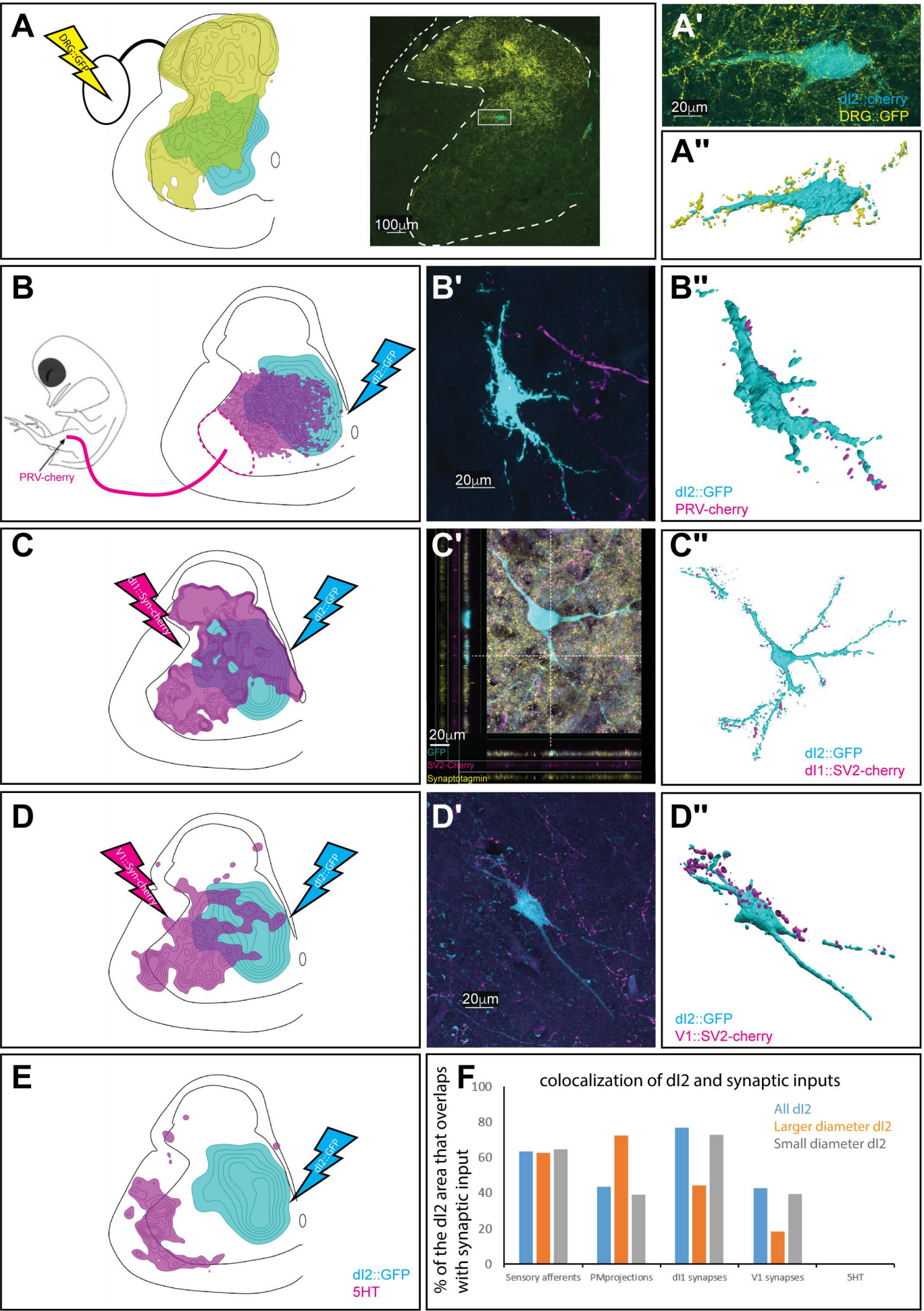
A
DRG::GFP
100µm
A'
20µm
dI2::cherry
DRG::GFP
A''
B
PRV-cherry
dI2::GFP
B'
20µm
B''
dI2::GFP
PRV-cherry
C
dI1::Syn-cherry
dI2::GFP
C'
20µm
GFP
SV2-Cherry
Synaptotagmin
C''
dI2::GFP
dI1::SV2-cherry
D
V1::Syn-cherry
dI2::GFP
D'
20µm
D''
dI2::GFP
V1::SV2-cherry
E
dI2::GFP
5HT
F
colocalization of dI2 and synaptic inputs
% of the dI2 area that overlaps with synaptic input
100
80
60
40
20
0
All dI2
Larger diameter dI2
Small diameter dI2
Sensory afferents
PMprojections
dI1 synapses
V1 synapses
5HT

Fig. 4

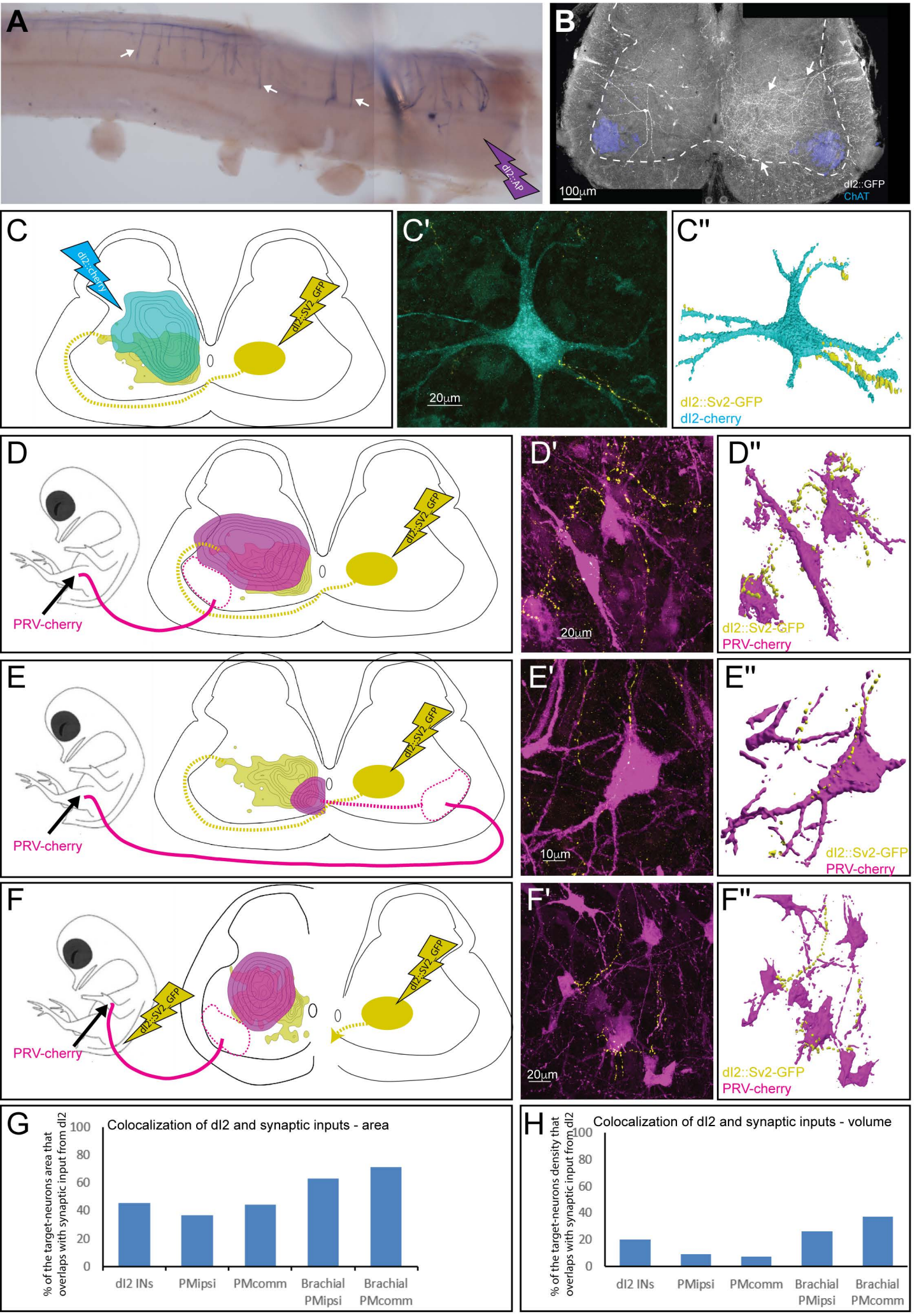
A
dI2::AP
B
100µm
dI2::GFP
ChAT
C
dI2::cherry
dI2::Sv2 GFP
C'
20µm
C''
dI2::Sv2-GFP
dI2-cherry
D
PRV-cherry
dI2::Sv2 GFP
D'
20µm
D''
dI2::Sv2-GFP
PRV-cherry
E
PRV-cherry
dI2::Sv2 GFP
E'
10µm
E''
dI2::Sv2-GFP
PRV-cherry
F
PRV-cherry
dI2::Sv2 GFP
dI2::Sv2 GFP
F'
20µm
F''
dI2::Sv2-GFP
PRV-cherry
G
Colocalization of dI2 and synaptic inputs - area
% of the target-neurons area that overlaps with synaptic input from dI2
100
80
60
40
20
0
dI2 INs
PMipsi
PMcomm
Brachial PMipsi
Brachial PMcomm
H
Colocalization of dI2 and synaptic inputs - volume
% of the target-neurons density that overlaps with synaptic input from dI2
100
80
60
40
20
0
dI2 INs
PMipsi
PMcomm
Brachial PMipsi
Brachial PMcomm

Fig. 5

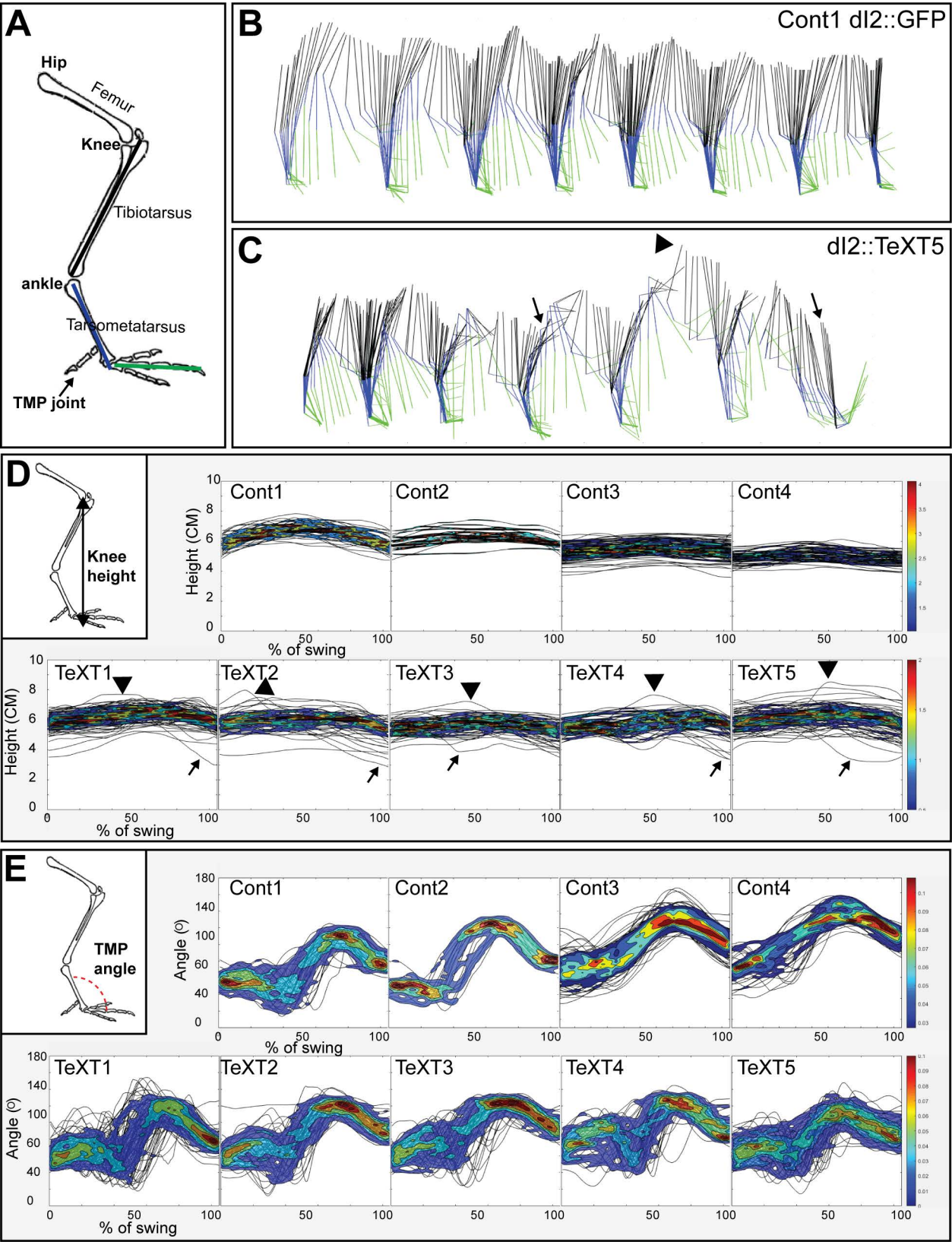
A
Hip
Femur
Knee
Tibiotarsus
ankle
Tarsometatarsus
TMP joint
B
Cont1 dl2::GFP
C
dl2::TeXT5
D
Knee height
Cont1
Cont2
Cont3
Cont4
Height (CM)
% of swing
TeXT1
TeXT2
TeXT3
TeXT4
TeXT5
E
TMP angle
Angle (°)

Fig. 6

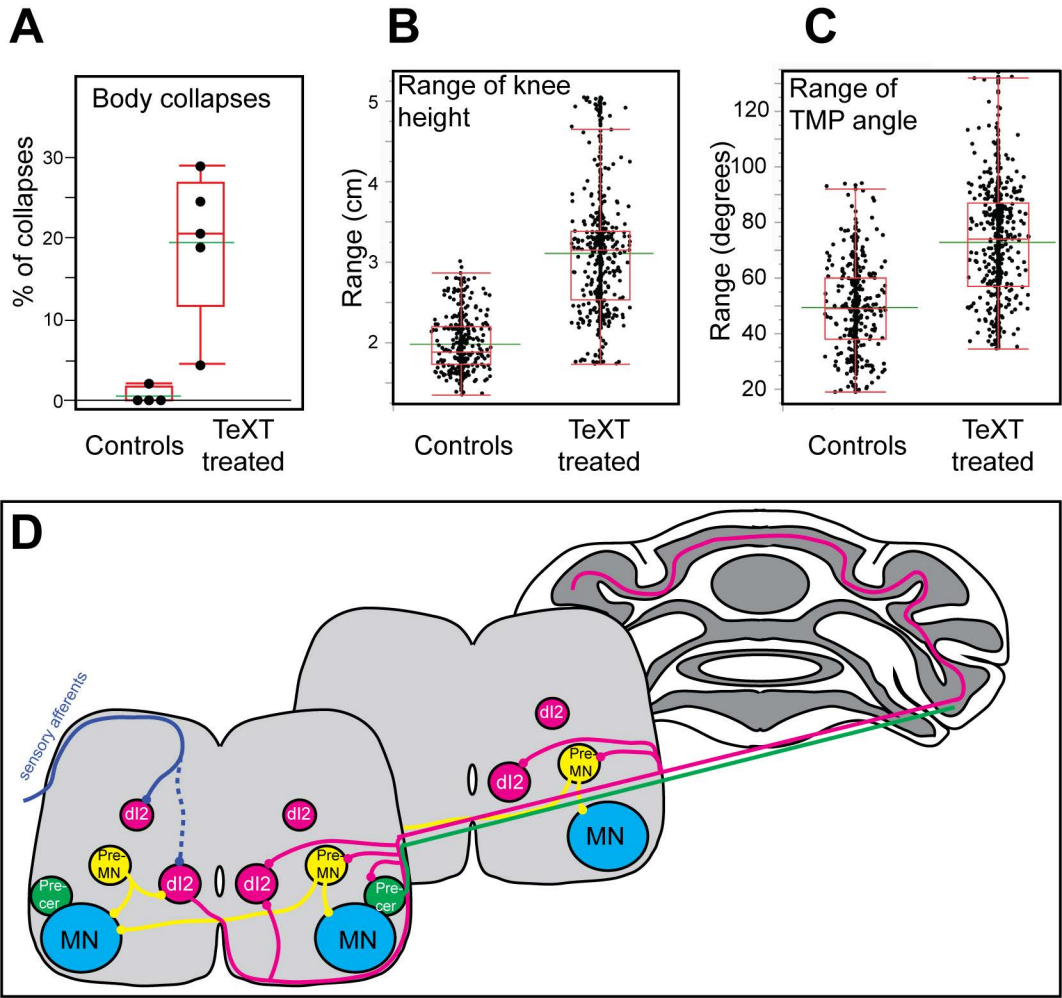
A
Body collapses
% of collapses
0
10
20
30
Controls
TeXT treated
B
Range of knee height
Range (cm)
2
3
4
5
Controls
TeXT treated
C
Range of TMP angle
Range (degrees)
20
40
60
80
100
120
Controls
TeXT treated
D
sensory afferents
dI2
Pre-MN
Pre-cer
MN